The ciliary kinesin KIF7 controls the development of the cerebral cortex by acting differentially on SHH-signaling in dorsal and ventral forebrain.

María Pedraza[1,$,#], Valentina Grampa[1,$], Sophie Scotto-Lomassese[1,$], Julien Puech[1], Aude Muzerelle[1], Azka Mohammad[1], Nicolas Renier[2], Christine Métin[1,&] and Justine Masson[1,&,##,*]

1. INSERM, UMR-S1270, Institut du Fer à Moulin, Sorbonne Université.
2. Institut du Cerveau et de la Moelle Épinière, Laboratoire de Plasticité Structurale, Sorbonne Université, INSERM U1127, CNRS UMR7225, 75013, Paris, France.

* Correspondence to justine.masson@inserm.fr
[$] These authors contributed equally to this work (co-first)
[&] These authors contributed equally to this work (co-last)
[#] Present address: Sharestist, Valencia, Spain.
[##] Present address: Université Paris Cité, NeuroDiderot, Inserm, F-75019, Paris, France.

Running title: *Kif7* deletion and cortical development

Keywords: kinesin, Sonic Hedghog pathway, mouse model, embryonic development, cortical projections, interneuron migration

ABSTRACT

Mutations of *KIF7*, a key ciliary component of Sonic hedgehog (SHH) pathway, are associated in humans with cerebral cortex malformations and clinical features suggestive of cortical dysfunction. KIF7 regulates the processing of GLI-A and GLI3-R transcription factors in a SHH-dependent manner both in humans and mice. Here, we examine the embryonic cortex development of a mouse model that lacks the expression of KIF7 (*Kif7 -/-)*. The cortex is composed of principal neurons generated locally in the dorsal telencephalon where SHH expression is low and inhibitory interneurons (cIN) generated in the ventral telencephalon where SHH expression is high. We observe a strong impact of *Kif7* deletion on the dorsal cortex development whose abnormalities resemble those of GLI3R mutants: subplate cells are absent, the intermediate progenitor layer and cortical plate do not segregate properly, and corticofugal axons do not develop timely, leading to a delayed colonization of the telencephalon by thalamo-cortical axons. These structural defects alter the cortical distribution of cIN, which moreover exhibit intrinsic migration defects resembling those of cyclopamine-treated cIN. Our results show that *Kif7* deletion impairs the cortex development in multiple ways, exhibiting opposite

effects on SHH pathway activity in the developing principal neurons and inhibitory interneurons.

INTRODUCTION

The primary cilium is a tiny microtubule-based organelle present on the surface of nearly all mammalian cell types including neurons, which functions as a signaling hub and transduces several signaling pathways comprising Sonic Hedghog (SHH), Wnt, Delta/Notch and mTOR pathways [1]. Primary cilium dysfunction causes pleiotropic diseases named ciliopathies. KIF7 is a ciliary kinesin responsible for the trafficking and the positive and negative regulation of the GLI transcription factors in the primary cilium of mammals [2]. Loss of function of KIF7 in the mouse has shown that KIF7 regulates (SHH) signalling by acting downstream of Smoothened (Smo) and upstream of GLI2 and GLI3 [3–7]. Studies in mice established that KIF7 activity is dependent on the expression level of SHH. In the absence of SHH, KIF7 localizes to the base of the primary cilium [5]. GLI factors are phosphorylated and addressed to the proteasome at the base of the primary cilium for degradation, leading to the formation of a cleaved and stable transcriptional repressor (GLI3-R). In the presence of SHH, KIF7 accumulates at the distal tip of the primary cilium [4,5] and associates with full length GLI2/3 that become transcriptional activators (GLI-A) [8].

Since 2011, ten studies have identified patients carrying mutations in the *KIF7* gene responsible of ciliopathies classified according to clinical features as hydrolethalus, acrocallosal, Joubert and Greig cephalopolysyndactyly syndromes [9–18]. MRI investigations revealed macrocephaly, ventricles enlargement and corpus callosum alterations. They also showed the characteristic hindbrain abnormalities observed in most ciliopathies such as molar tooth sign (MTS) and cerebellar atrophy. Patients also presented with mild but frequent cortical malformations as well as neurodevelopmental delay, intellectual disability and seizures [10,13,16,19] which indicate cortical abnormalities.

In physiological conditions, the proper activity of the cortex relies on the excitatory/inhibitory balance i.e. on the ratio, positioning and connectivity of excitatory glutamatergic (principal neurons, PN) and inhibitory GABAergic interneurons (cIN), generated from progenitors in the dorsal and ventral telencephalon, respectively. The cortical neurons of dorsal and ventral origin each migrate towards the developing cortex, the so-called cortical plate (CP), according to a specific timeline allowing the establishment of proper connections in the CP.

SHH plays a central role in establishing the dorso-ventral patterning of the forebrain, and in regulating the proliferation and differentiation of cortical progenitors of dorsal and ventral

origins. At early embryonic stage, the ventral expression of SHH orchestrates the ventro-dorsal [20,21] and medio-lateral [22] regionalization of the mouse forebrain and the differentiation of ventral cell types [20]. *Shh* ablation performed after forebrain patterning alters the specification of distinct subgroups of GABAergic interneurons [23–26]. Interestingly, conditional ablation of *Shh* and *Smo* in the embryonic cortex reduces the proliferation of dorsal progenitors [27], demonstrating a minimal SHH expression in the dorsal telencephalon, even before birth [28]. Beside its role on proliferation and specification, SHH also controls the migration of interneurons to the cortical plate [29–33]. In the embryonic telencephalon, GLI transcription factors mediate SHH signals in complex and specific ways. The three GLI factors identified in mammals are expressed in the mouse forebrain: GLI1 along the source of SHH in the ganglionic sulcus, and GLI2 and GLI3 dorsally to the SHH source [26,34,35]. GLI1 acts uniquely as a pathway activator whereas GLI2 and GLI3 can be processed in transcriptional activators or inhibitors in the primary cilium. However, both GLI1 and GLI2 function primarily as transcriptional activators in response to SHH activity in the ventral forebrain [35]. Nevertheless, GLI1 and GLI2 mutants show mild phenotypes [36,37] and GLI2 seems required to transduce high level SHH signals in mice [38]. In contrast, the development of the dorsal cortex, where principal excitatory neurons differentiate, depends mainly on the expression of the GLI3-R repressor, revealing low cortical expression of SHH [39,40]. Following patterning, Gli3R/A ratio remains critical for specifying the fate of cortical progenitors and regulating cell cycle kinetics [41,42].

Previous studies investigated the mechanisms underlying the corpus callosum agenesis in patients with *KIF7* mutation using *Kif7* knock-out (*Kif7* -/-) mice [43] and the consequence of KIF7 knock down on cortical neurogenesis in principal cells electroporated with *Kif7* shRNA [44]. Nevertheless, the influence of developmental abnormalities associated with ciliopathies on the cortical cytoarchitecture is poorly understood. Given the crucial role of KIF7 in regulating the GLI pathways and the important role of Gli3-R and GLI2/3-A in regulating the early developmental stages of the dorsal and ventral telencephalon, respectively, we examined here the cortical development, the establishment of long distance projections with the thalamus and the migration of GABAergic interneurons (cIN) in *Kif7* -/- mice. We focused at embryonic stage E14.5, a key period in corticogenesis when the cortical plate begins to form and cIN start to invade the developing cortex. The influence of abnormal SHH signaling in *Kif7* -/- mice on the migratory behavior of cIN was investigated by comparing the migration of cIN in living *Kif7* -/- cortical slices and in control slices treated with pharmacological activator and inhibitor

of the SHH pathway. We moreover determined the local distribution of the SHH protein in the embryonic cortex.

Our results show developmental defects leading to permanently displaced neurons, abnormal formation of cortical layers and defective cortical circuits that could be responsible for epilepsy and/or intellectual deficiency in patients carrying *KIF7* mutation [9–18].

RESULTS

Kif7 knock-out mice as a model to investigate the structural cortical defects that could lead to clinical feature in patients carrying KIF7 mutation.

The *KIF7* gene is located on chromosome 15 in human and encodes a 1343 aa protein containing in the N-terminal part, a kinesin motor domain and a GLI-binding domain followed by a Coiled-coil region and in the C-terminal part, a Cargo domain able to bind a diverse set of cargos [47]. Table 1 summarizes the clinical features associated with mutations targeting either the kinesin or GLI binding domain in the N-terminal part of the protein, the Coiled-coil domain, or the N-terminal Cargo domain. Interestingly, various mutations are associated with the same clinical picture, suggesting that *KIF7* mutations, whatever their nature, could lead to protein loss of function, for example by altering the protein structure and solubility as proposed by Klejnot and Kozielski (2012). All patients carrying mutation in the *KIF7* gene have developpemental delay (DD) and intellectual deficit (ID) associated with classical defects of ciliopathies such as ventricle enlargement, macrocephaly, corpus callosum (CC) agenesis and molar tooth sign (MTS). Some patients have anatomical cerebral cortex defects as poor frontal development, atrophy, pachygyria and heterotopia [9,17,18,49] that could participate not only to DD and ID but moreover to seizure as observed in a quarter of patients. In this context, we used a murine model in which the *Kif7* gene had been deleted (*Kif7* -/-) [3] to investigate the consequence of KIF7 loss of function on the cortex development. *Kif7* -/- mice have been previoulsy characterized as dying at birth with severe malformations, including exencephaly in a third of the mutants, skeletal abnormalities (digits and ribs), neural tube patterning defects, microphtalmia, lack of olfactory bulbs and CC agenesis [3,4,15]. In the present study, the KIF7 loss of function was analyzed in a mouse strain with a mixed genetic background in which exencephaly at E14.5 was observed at the same frequency in *Kif7* -/- and control embryos. As previously reported, E14.5 *Kif7* -/- embryos displayed microphtalmia (Fig. 1A, black arrow) and polydactily (not illustrated). Interestingly, skin laxity previously reported in ciliopathic patients [50,51] was observed in all mutants (Fig. 1A, white arrow). Comparison of brains from *Kif7* -/- embryos and control littermates at E14.5 revealed that *Kif7* -/- could be distinguished

by the absence of olfactory bulbs (Fig. 1B, white arrows), a thinning of the dorsal cortex allowing the lateral ventricles to be seen through (Fig. 1B, black arrow and Fig. 1C1) and a prominent diencephalon (Fig. 1C1).

Kif7 invalidation alters the development of the cortex at E14.5.

Analyses performed on rostro-caudal series of frontal sections (Fig. 1C1) confirmed that the brain of E14.5 *Kif7* -/- embryos exhibited enlarged lateral ventricles (Fig. 1C2) and thinned dorsal cortex (Fig. 1C3) resulting however in unchanged total width and height of the telencephalon (Fig. 1C4,5). KIF7 depletion in E10.5-E11.5 mouse embryos was reported to alter the dorso-ventral patterning of the medial forebrain [15], in line with the decreased expression of the transcriptional repressor GLI3R [3,4]. GLI3 loss of function [52,53] has been associated with an abnormal dorso-ventral patterning of the telencephalon. We confirmed here the decreased expression of GLI3R in the cortex of *Kif7* -/- embryos (Fig. S1). However, the frontier of expression of GSH2 (Fig. 1D1) and TBR2 (Fig. 1D2), two transcription factors expressed in the ventral and dorsal telencephalon respectively, was preserved in the pallium-subpallium boundary (PSB) at E14.5 in *Kif7* -/- embryos, suggesting a rather normal dorso-ventral patterning of the telencephalic vesicles in their lateral side.

The thinning of the dorsal cortex of E14.5 *Kif7* -/- embryos convinced us to examine the structural organization of the cortex of *Kif7* -/- embryos. At E14.5, the mouse cortex can be described as a stack of three specialized domains: i) the upper/superficial cortical layers containing post-mitotic cells generated in the proliferative zones of the cortex, including TBR1(+) post-mitotic neurons located in the cortical plate (CP); ii) the deep proliferative layers, ventricular and subventricular zones (VZ and SVZ, respectively), located along the lateral ventricle; iii) the intermediate zone (IZ) located between the CP and the proliferative layers, which hosts the radially and tangentially migrating neurons and growing axons. In control embryos, TBR1(+) cells formed a rather regular, radially organized CP surrounded by two thin continuous layers of MAP2(+) neurons located in the upper marginal zone (MZ) and the bottom subplate (SP) respectively (Fig. 2A, left). In *Kif7* -/- embryos, the TBR1(+) CP cells appeared more clustered and the thickness of the upper MAP2(+) layer was extremly irregular. MAP2(+) cells were no longer observed below the CP in the dorsal cortex (Fig. 2A, arrow on right panel). Moreover, focal heterotopia characterized by an abnormal accumulation of TBR2(+) cells were observed in the dorsal or lateral cortex of *Kif7* -/- embryos, either at the ventricular or pial surface (Fig. S2). TBR2 labels the intermediate progenitors (IP) of principal cells, which normally form a dense layer in the SVZ of the cortex (Fig. 2B1, left). Beside sporadic

heterotopia, the TBR2(+) layer constantly showed an abnormal positioning in the dorsal cortex of *Kif7* -/- embryos. TBR2(+) cells indeed reached the brain surface (Fig. 2B1, arrow) where they mixed up with post-mitotic TBR1(+) cells instead of keeping a minimal distance with TBR1 cells as observed in control brains (Fig. 2B2, arrow) and in the lateral cortex of *Kif7* -/- brains (Fig. 2B2). Therefore, intermediate progenitors and post-mitotic neurons no longer segregated in the dorsal cortex of *Kif7* -/- embryos and no IZ was observed (Fig. 2B2, white arrow).

The loss of Kif7 alters the connectivity between the cortex and the thalamus at E14.5.

The intermediate zone (IZ) hosts the radially and tangentially migrating neurons and comprises the growing cortical and thalamic projections [54]. Corticofugal axons develop from early stages: the trailing process of post-mitotic neurons migrating radially to the CP first elongates tangentially in the IZ and then differentiates as an axon [55,56]. We thus examined whether the defaults observed in the CP and the lack of IZ in the dorsal cortex of *Kif7* -/- embryos did associate with developmental abnormalities of the corticofugal projection. We labeled corticofugal axons by inserting small crystals of DiI in the dorsal or lateral cortex in E14.5 paraformaldehyde fixed brains. After DiI had diffused along corticofugal axons, we analyzed labeled axons on coronal sections. In both control and *Kif7* -/- brains, CP neurons located in the dorsal or lateral cortex extended axons below the CP toward the PSB (Fig. 3A). DiI injections in the dorsal cortex of control and *Kif7* -/- brains (Fig. 3A1) labeled much less axons than injections in the lateral cortex (Fig. 3A2,A3) according to the latero-medial gradient of cortical development. Very remarkably, the cortical bundles labeled from similar cortical regions were always much smaller in *Kif7* -/- than in wild type brains (Fig. 3A, compare right and left columns). Whereas dorsal injections labeled large bundles crossing the PSB in control brains, only a few axons reached the PSB in *Kif7* -/- brains (Fig. 3A1), showing that corticofugal axons growth was severely hampered in the dorsal cortex of *Kif7* -/- embryos. Corticofugal axons labeled from lateral injection sites in control brains crossed the PSB, extended within the embryonic striatum and continued medially in the internal capsule (IC) where they met thalamic axons retrogradely labeled from the lateral cortex (Fig. 3A3, left panel). In *Kif7* -/- embryos, lateral injections labeled axons that either spread in the striatum (Fig. 3A2, right panel) or extended ventrally to the cerebral peduncle (Fig. 3A3, right panel, white arrow), a trajectory never observed in control brains. Moreover, no thalamic axons were retrogradely labeled from the lateral cortex. To identify the trajectory of thalamic axons in *Kif7* -/- embryos, we immunostained coronal sections of E14.5 brains with antibodies against the Netrin G1a (NG1a),

an early marker of thalamocortical axons (TCA, Fig. 3B) [57]. At E14.5, in both control and *Kif7* -/- brains, NG1a antibodies labeled a large population of dorsal thalamic neurons (Fig. 3B). In control brains, thalamic axons made a right angle turn to join the IC. Then they extended to the PSB and some axons entered the lateral cortex (Fig. 3B, left panel). In *Kif7* -/- embryos, most thalamic axons stopped their course at the exit of the diencephalon (Fig. 3B, white arrow in right panel) while some of them formed a short and thick bundle oriented ventrally to the surface of the basal telencephalon (Fig. 3B, white arrow in right panel). No evident structural defect could be observed at the telo-diencephalic junction in *Kif7* -/- brain (Fig. S3A). Given the complexity of the trajectory of NG1a thalamic axons, we immunostained thalamic axons in whole brains and imaged them after transparisation using a light-sheet microscope. Reconstruction and three-dimension analysis of labeled projections confirmed that thalamic axons made a sharp turn to reach the IC and then navigated straight to the PBS in control brains (Fig. 3C, Fig. S3B and Movie S1). In contrast, most thalamic axons stopped their course after leaving the diencephalon in *Kif7* -/- embryos, and formed two large bundles, one oriented to the IC (Fig. 3C, white star and Movie S2) and another one oriented caudally (Fig. 3C, white arrow, Fig. S3B and Movie S2). This last projection was never observed in control brains (Movie S1). The present analysis thus identified impaired trajectories of corticofugal and thalamo-cortical projections at E14.5 in the basal forebrain of *Kif7* -/- animals, suggesting impaired axonal guidance mechanisms in the basal forebrain.

Kif7 invalidation alters the cortical distribution of cIN at E14.5.

Because cIN are born in the basal forebrain and likely depend on contact/functional interactions with pioneer corticofugal projections for the first stages of their migration [58,59], we also examined the distribution of cIN in the developing cortex of *Kif7* -/- animals. cIN are generated outside of the cortex, in the medial and caudal ganglonic eminences (MGE, CGE) and preoptic area (POA) of the ventral forebrain. They enter the lateral cortex at E12.5 - E13.5, depending on mouse strains, and colonize the whole cortex by organizing two main tangential migratory streams, a superficial one in the MZ, and a deep and large one in the lower IZ/SVZ [60,61]. Intermediate cortical progenitors of the SVZ and meninges strongly express *CxCl12* mRNA [62], coding for a chemokine essential for cIN to recognize their tangential pathways of migration in the developing cortex. CXCL12 promotes the tangential progression of cIN in the developing cortex and prevents the premature occurrence from switch to tangential to radial mode of migration that is required for cIN to colonize the CP [62–65]. We analyzed the expression of *CxCl12* mRNA in the cortex of mutant embryos using *in situ* hybridization experiments at

E14.5, a stage when TBR2(+) SVZ cells show defective positioning in the dorsal cortex of *Kif7* -/- embryos. In control brains, *CxCl12* mRNA showed a latero-medial gradient of expression in the SVZ, which ended at the frontier with the hippocampus. In contrast, *CxCl12* mRNA was no longer expressed in the dorsal cortex of *Kif7* -/- embryos (Fig. 4A, black arrow), in the region where TBR2(+) cells starts to position at the brain surface (Fig. 4B1). We thereafter analyzed the cortical distribution of Tomato(+) MGE-derived cIN at E14.5 in control Nkx2.1-Cre;Rosa26-TdTomato transgenic embryos and in *Kif7* -/-, Nkx2.1-Cre;Rosa26-TdTomato transgenic mutant embryos (Fig. 4B and see methods). The latero-medial extent of both the superficial and deep tangential migratory streams was significantly shortened in *Kif7* -/- brains as compared to control brains (Fig. 4B1, white arrows). Very remarkably, the cIN deep tangential stream stopped in the region where the layer of TBR2(+) cells started its abnormal switch to the surface of the cortex (Fig. 4B1, white arrows) and did not colonize the dorsal cortex (Fig. 4B2). In addition, cIN presented an altered radial distribution in the cortex of *Kif7* -/- embryos (Fig. 4C). The superficial migratory stream was thinner and denser in the MZ of *Kif7* -/- embryos as compared to control (Fig. 4C1, left panel in C2) and the distance between the superficial and deep tangential migratory streams was significantly diminished in the lateral cortex of *Kif7* -/- mutants (Fig. 4C2). This decrease is in agreement with the reduced corticofugal projections identified in *Kif7* -/- mutants, as these axons navigate tangentially in the IZ. The reduced latero-dorsal distribution of cIN and their abnormal distribution in the cortical thickness reflected structural and molecular abnormalities identified in the cortex of *Kif7* -/- embryos. To verify if migratory defaults proper to *Kif7* -/- cIN could moreover contribute to their abnormal distribution in the cortex of *Kif7* -/- embryos, we analyzed the migration of cIN in living cortical slices.

Kif7 invalidation and SHH pathway activity both affect the migratory behavior of cIN in cortical slices.

The forebrain of E14.5 Nkx2.1-Cre;Rosa26-TdTomato transgenic embryos exhibiting or not a *Kif7* deletion (control and *Kif7* -/-, respectively) were sliced coronally to image the cortical migration of cIN by time-lapse video-microscopy (Fig. 5). In control slices (Fig. 5A1, Supplementary Movie S3), fluorescent cIN migrated tangentially from the PSB to the dorsal cortex in two main pathways, a superficial one in the MZ and a deep one in the lower IZ/SVZ. All along these pathways, some cIN operated a tangential to oblique/radial migration switch to colonize the CP. Since high cell density in the MZ prevented a dynamic monitoring of tangentially migrating cells, cells migrating in the MZ were not analyzed in this study.A large

proportion of cells imaged during the recording session (59.3 %), either maintained tangentially oriented trajectories in the deep stream (28.7 %, red trajectories in Fig. 5A1, left column of Fig. 5A2 and Fig. 5A3) or reoriented to the CP along oblique (and less frequently radial) trajectories (30.6 % green trajectories in Fig. 5A1, left column in Fig. 5A2). A majority of cells reached the CP surface and remained there. A smaller proportion of cIN moved from the deep stream to the opposite - ventricular- side of the slice (11.7%, blue trajectories in Fig. 5A1, left column in Fig. 5A2 and Fig. 5A3). In the VZ, deep stream, and CP, a minimal proportion of cIN (3.6 %) moved very short distances or remained immobile (dark colors in the left column of Fig. 5A2). A significant proportion of cIN (15.6 %) migrated radially, traveling all over the cortex thickness and frequently inverting their polarity in the MZ or at the ventricular surface (pink trajectories in Fig. 5A1, left column in Fig. 5A2 and Fig. 5A3). Finally, 8 % (orange) of the recorded cIN moved backward to the ventral brain and 1.7 % of them (grey) did not show any specific directionality or layer specificity and were classified as chaotic (Fig. 5A1, left column in Fig. 5A2 and Fig. 5A3). A large majority of cIN presented a characteristic saltatory behavior, alternating stops and fast moves [66]. Analyses of resting and moving phases of the largest cIN population recorded in the deep stream and/or moving to the CP are illustrated in Fig. 5B1-3 (left column of histograms). The trajectories followed by cIN in the cortical slices of *Kif7* -/- embryos dramatically differed from those in control slices (Fig. 5A2,A3 and Supplementary Movie S4 compared to S1). The number of cIN migrating tangentially in the deep migratory stream and moving to the CP from the deep stream dropped drastically (17.8 % as compared to 59.3 % in control slices), instead, they were immobile (35.7 % as compared to 3.6 % in control slices) especially in the SVZ/lower IZ. Almost the same proportion of cIN moved to the ventricle and to the CP (10.2 % and 13.9 %, respectively, as compared to 11.7 % and 30.6 % in control slices) suggesting that the radial asymmetry of cortical slice was lost for *Kif7* -/- cIN. The proportion of cIN migrating radially across cortical layers remained similar as in control slices (17.2 % versus 15.6 % in control) but the proportion of cIN with chaotic trajectories strongly increased (7.8 % versus 1.7 % in control slices, Fig. 5A2, second column, Fig. 5A3). Another major change observed in the *Kif7* -/- cortical slices was a significant decrease of the migration speed (excluding immobile cIN) (Fig. 5B1) and an abnormal saltatory behavior, with less frequent but longer resting phases than in control slices (Fig. 5B2,B3). Of note, trajectories were analyzed at E14.5 in the lateral and latero-dorsal cortex where *CxCl12* mRNA was observed in both control and *Kif7* -/- embryos (Fig. 4A). Because CXCL12 is a potent chemoattractant for migrating cIN, the very large proportion of immobile cIN recorded in the CXCL12-expressing deep stream of *Kif7* -/- slices was suggestive of intrinsic migratory defaults

of *Kif7* -/- cIN. *Kif7* ablation has been shown to induce either transcriptional SHH signaling activation by inhibiting the processing of GLI3 in GLI3-R repressor, or transcriptional SHH signaling inhibition by inhibiting the positive impact of KIF7 on the GLI1/2 dependent SHH signaling [3]. We thus examined whether the acute application of drugs able to either promote or inhibit the SHH signaling could induce in wild type cIN migratory defaults resembling those of cIN in *Kif7* -/- cortical slices. SHH application on control slices minimaly affected the trajectories of cIN (Fig. 5A2, compare left and right columns, Fig. 5A3), except an increased proportion of cIN migrating radially (29 % compared to 15.6 % in control slices) at the expense of cIN migrating from the deep stream to the CP (20.8 % instead of 30.6 % in control slices). In addition, cIN moving radially across the cortical layers no longer stopped in the CP and frequently moved backward to the VZ (Fig. 5A2,A3, Supplementary Movie S5). The frequency of chaotic trajectories (grey, Fig. 5A2) did not increase, and the migration speed of cIN was slightly decreased compared to control slices (Fig. 5B1). Main dynamic alteration of SHH treated cIN was the increased duration of resting phases (Fig. 5B2,B3). On the contrary, application of the SHH pathway inhibitor cyclopamine strongly altered cIN trajectories (Fig. 5A2,A3). For example, the proportion of immobile cIN and of cIN moving short distance reached 33.7 % as compared to 3.6 % in control slices (Fig. 5A2). Most immobile cells in cyclopamine treated slices were located in the deep stream, and only few cIN switched from the deep stream to the CP at the benefit of cIN migrating backward to the ventral brain. Therefore, inhibiting the SHH pathway mainly affected the ability of cIN to move tangentially in the deep stream and to switch to the CP (Fig. 5A2,A3, Supplementary Movie S6),. Globally, cIN trajectories in cyclopamine treated slices recalled the trajectories of cIN in *Kif7* -/- cIN (Fig. 5A2, compare columns 2 and 3), suggesting that *Kif7* ablation resembled the cyclopamine-mediated SHH pathway inhibition. Nevertheless, whereas the migration speed of *Kif7* -/- cIN was significantly decreased in the deep tangential pathway and not in CP, cyclopamine application decreased the migration speed only in the CP (Fig. 5B1). The strong influence of cyclopamine on the cortical migration of cIN led us to determine the distribution of the endogenous activator SHH in the developing cortex.

Distribution of Shh mRNA and SHH protein in the E14.5 cortex.

Shh mRNA is strongly expressed by the mantle zone of the ganglionic eminences (MGE, CGE) and POA during the time cIN differenciate [24,56] but its level of expression in cIN after they reach the cortex is controversial [29,31,67]. We thus reexamined *Shh* mRNA expression in forebrain and SHH protein distribution in cortical layers. *In situ* hybridization (ISH) experiments performed

at E13 confirmed the strong expression of *Shh* mRNA in the ventral forebrain, especially in the SVZ and mantle zone of the MGE (Fig. 6A1,6B1) in agreement with the SHH-dependent *Gli1* mRNA expression in a VZ subdomain of the MGE [68]. In contrast, *Shh* transcripts were bearly detectable in the cortex. Using RNAscope, whose sensitivity and spatial resolution is higher compared to standard ISH, we re-examined the expression pattern of *Shh* mRNA at E14.5. In the ventral forebrain, RNAscope *Shh* transcript detection showed similar expression pattern as ISH (Fig. 6A2,B2). In addition, the expression domains of *Shh* mRNA and *Lhx-6* mRNA, a cIN marker, overlapped in the mantle zone of the MGE (Fig. 6A2). In the cortex, some cells oriented either radially in the VZ/SVZ or tangentially in the tangential migration pathways expressed *Shh* mRNA at a very low level (one or two dots versus large cluster in the MGE) (Fig. 6A2). In the tangential migration streams where a large number of cIN expressed *Lhx-6* mRNA (Fig. 6C1,C2), cIN that co-expressed *Lhx-6* and *Shh* mRNA represented near 5 % of cIN expressing *Lhx-6* transcript (Fig. 6C3).

Antibodies that recognize the N-ter part of SHH [SHH-Nter, e.g. "activated" SHH [69]] strongly labeled brain regions known to strongly express SHH [67,70,71], such as zona limitans intrathalamica and the lateral walls of the third ventricle at E12.5 (Fig. S4), and the choroid plexus at E14.5 (Fig. 6D1), validating the SHH-Nter antibodies used here. At E14.5, SHH-Nter antibodies immunostained bright tiny dots aligned radially in the VZ/SVZ, and tangentially in the IZ. In the CP, dots were again radially aligned and some CP cells presented a rather diffuse cytoplasmic staining, which was not observed in the bottom layers (Fig. 6D2). We observed no particular SHH enrichment in the lower IZ/SVZ where cIN migrate, suggesting that their contribution to the cortical pattern of SHH expression was minimal. Moreover, large dots were observed in the subpallium at the ventricular angle (Fig. 6D4). Together, our ISH and immunostaining experiments showed that the cortical SHH protein has probably an extrinsic origin as previously described at the early stage of cerebellum development (Huang et al, 2010).

Ontogeny of Kif7 mutant brain developmental defects.

After E14.5, the cortex of *Kif7* -/- embryos continued to develop. Analyses performed at E16.5 showed that cIN continued to migrate tangentially and reached the dorsal cortex in *Kif7* -/- embryos (Fig. 7A). Nevertheless, the tangential migration of cIN to the dorso-medial cortex remained delayed in *Kif7* -/- embryos with regard to the tangential migration of cIN in control embryos. *Kif7* -/- cIN failed to reach the hippocampus identified by the presence of TBR2(+) cells, as observed in control brains (compare left and right panels in Fig. 7A). At E16.5, NG1a(+) thalamic axons colonized the whole medial and rostral cortex, in both control and *Kif7*

-/- embryos (Fig. 7B). Nevertheless, thalamic axons were less dense in *Kif7* -/- than in control cortex and exhibited abnormal trajectories (Fig. 7C) toward the cortical plate. Analyses performed in a surviving P0 animal (Fig. S5) revealed an abnormal distribution of cIN in the cortical plate, with a decreased density in the bottom layers, which were moreover thinner than in control brains, as illustrated by CTIP2(+) staining (Fig. S5A). The cortical distribution of thalamic axons was extremely perturbed in *Kif7* -/- brains: a dense bundle of NG1a(+) fibers ran below the cortical plate to the dorsal cortex and failed to invade the CP (Fig. S5B).

DISCUSSION

Our aim in the present paper was to better understand the developmental origin of functional abnormalities (e.g. epilepsy, cognitive deficits, …) in cortical circuits of human patients with *KIF7* mutations by characterizing the developmental abnormalities of the cerebral cortex in a *Kif7* -/- mouse model. We show that *Kif7* ablation affects the development of the two populations of cortical neurons, cortical plate neurons and GABAergic interneurons, in specific and distinct ways, accordingly with their dorsal and ventral origin in the telencephalon. The alterations of the CP development (lack of most subplate cells in the dorsal cortex, and delayed corticofugal projection) are remiscient of defaults previously described in GLI3 null mutants that lack most subplate neurons and pioneer cortical projections [72]. And the abnormal distribution of *Kif7* -/- cIN in the developing cortex indeed reflects the structural and functional alterations of cortical layers on which cIN migrate (e.g. abnormal CXCL12 expression in the SVZ). However, we identify moreover migration defaults of *Kif7* -/- cIN that recall those of wild type cIN treated with the SHH pathway inhibitor cyclopamine, suggesting that the SHH pathway activity is inhibited in *Kif7* -/- cIN. *Kif7* ablation thus alters specifically and differently the SHH pathway activity in CP and cIN subpopulations, in agreement with their dorsal or ventral origin.

<u>*Kif7* knock-out mice as a model to study the effect of mutation in the *KIF7* gene in human.</u>

The deletion of *Kif7* gene in mice leads to lethality the first day of life, but up to birth, the brain develops and a previous study demonstrated that *Kif7* mutant mice was a good model to dissect the mechanism that led to corpus callosum agenesis in patients [15]. All patients carrying mutation in the *KIF7* gene on both alleles have developmental delay/intellectual disability (ID) and some have seizures. Investigations on cerebral malformation by MRI have shown that some of them have alterations in the cerebral cortex including cortical atrophy [9,10,18] and pachygyria [17]. Detecting defects in the cerebral cortex is more demanding in MRI quality images that corpus

callosum agenesis or molar tooth sign, we can speculate that the number of patients with cerebral cortex defects was underscored. Malformations of cortical development was recognized as causes of ID [73] and epilepsy [74] and the cellular defects underlying these pathologies could imply defects in cell proliferation, neuronal migration and differenciation that lead to improper excitatory/inhibitory balance, connectivity into the cortex or of the cortex with other brain structures. The mechanism of action of KIF7 to transduce SHH ciliary dependent signaling has been debated. It has been accepted that SHH activates KIF7 binding to microtubules and its accumulation to the tip of the cilium, making the kinesin motor domain the most essential domain for SHH transduction. A more recent study proposed that KIF7 is an immobile kinesin translocated to the cilium tip after SHH binding by a complex KIF3A/Kif3B/KAP [75] suggesting that domains in the *KIF7* gene essential to its function are more complex. This could explain why any mutation, even point mutation in the Coiled-coil domain or in C-terminal part of the KIF7 protein induces clinical feature as severe as when mutation led to a highly truncated protein. Another explanation is that any mutation causes unproper folding of the protein inducing its degradation by the proteasome.

<u>KIF7 loss of function alters the cerebral cortex organization and the connectivity between the cortex and thalamus.</u>

In the mouse embryo, GLI3 plays a major role in patterning the dorsal telencephalon and in regulating the proliferation and differenciation of cortical neurons [40–42]. The *Kif7* knock-down that likely decreases GLI3R level leads to a decrease of apical radial progenitors and basal IP divisions, and of neuronal differenciation [44]. In fibroblasts isolated from lung of patients carrying *KIF7* mutation and in E11.5 *Kif7* -/- whole embryo, the processing of GLI3-full length in GLI3-R is decreased and GLI-A increased leading to over-SHH signaling [3,49]. Our study demonstrates that the level of GLI3-R was decreased in the developing cortex of the *Kif7* -/- embryos, whose layering of principal neurons was altered and exhibited sporadic heterotopia and delayed connectivity between the cortex and the thalamus. Heterotopia have been observed in one patient [17] and we found cortical heterotopia in some *Kif7* -/- brains. Cortical heterotopia is not a landmark of ciliopathy but were detected in a Joubert syndrom patient carrying a mutation in the *CELSR2* gene coding for a planar cell polarity protein [76] essential for neural progenitor cell fate decision, neural migration, axon guidance and neural maturation [77,78]. In the patient as in the mice model, the heterotopia are focal and may have been missed in other patients. They nevertheless emphasize the mistrafficking of principal cells in KIF7 depleted brain. Although disorganized thalamo-cortical connectivity had never been reported in patients

with *KIF7* mutation or in patients with ciliopathy, thalamocortical connectivity is essential for cognitive performances in young infants [79] and its alteration leads to neurodevelopemental delay and later cognitive deficits [80]. Moreover, a link beween ciliary function, cortex development and connectivity with the thalamus had been previously identified in mutant mice lacking planar cell polarity proteins CELSR2 and FZD3. These mice display ciliary defects and an abnormal development of tracts between the thalamus and the cortex leading to an hypotrophy of the intermediate zone where thalamo-cortical and corticofugal axons navigate [81,82].

Extra-cortical origin of SHH

Beside its major function in forebrain patterning [20,40], SHH moreover regulates the embryonic and perinatal cerebral cortex development [27,28]. The origin of the morphogen in this brain structure remains obscure. In agreement with a recent set of data from Moreau et al. [83], we showed that cIN born in the MGE or POA no longer express SHH after they reach the developing cortex. In addition, the level of local *Shh* mRNA synthesis was extremely low in the cortex at E14.5. In contrast, SHH protein was detected in immunoposive dots distributed throughout the cortex. Dots aligned radially in the VZ and CP, and tangentially in the IZ. This cortical distribution is compatible with an extrinsic origin of SHH and transventricular delivery as described in the cerebellar ventricular zone [84]. SHH is indeed present in the cerebrospinal fluid and likely secreted by the plexus choroid, since *Shh* mRNA is expressed in the choroid plexus of mice from E12 to E14.5 [85]. Accordingly, we showed here that the choroid plexus of the lateral ventricles was strongly immunopositive for SHH at E14.5. Interestingly, the CDO/BOC co-receptor - that favors SHH transport - was also detected along radially oriented structures by immunostaining in the mouse embryonic cortex (not illustrated). SHH could thus be transported away from the ventricular zone and/or meninges in vesicular structures able to diffuse accross the cortical thickness. Accordingly, it has been shown that SHH transport needs ESCRT-III member protein CHMP1A [13] and SHH related proteins are found in exosomes secreted from Caenorhabditis elegans epiderman cells [86], Drosophila wing imaginal discs [82], chick notochord cells and human cell lines [87]. How SHH is transported thoughout the cortex should be further explored. It has already be shown that SHH is present in multivesicular bodies, in neurites and filipodia in the post natal hippocampus and cerebellum, and in vesicles located inside and outside of hippocampal neurons in culture [88].

Kif7 deletion leads to defects in cortical interneuron migration

The defects induced by gene mutations responsible of primary cilium dysfunction, including *Kif7* deletion, have been examined in principal cells born in the dorsal telencephalon, which organize the cortical layers [89,90]. However, the cIN are born ventrally and migrate to the cortex during the embryonic development. Their primary cilium is functional and can transduce local SHH signals to influence their directionality, especially the tangential to radial reorientation of their trajectories toward the cortical plate [29]. In the present study, we showed that acute SHH application on control cIN slightly increased the percentage of radially migrating cIN. In contrast, cyclopamine that inhibited the SHH pathway blocked the migration of a large population of cIN in the deep cortical layersdemonstrating that endogeneous cortical SHH is likely to activate the SHH pathway in migrating cIN to control their trajectories. Since *Kif7* -/- cIN showed a migratory behavior that recalled the migratory behavior of cyclopamine treated control cIN, we concluded that SHH signaling was inhibited in *Kif7* -/- cIN. By consequence, we propose that *Kif7* -/- cIN, which differentiate in a ventral telencephalic domain expressing high SHH level, present reduced Gli-A signaling, e.g. decreased SHH signaling. In addition to this cell autonomous defect that impairs cIN migration, the colonization of the dorsal cortex by *Kif7* -/- cIN could be delayed due to the decreased dorsal expression of CXCL12 in *Kif7* -/- embryos [62,91].

In conclusion, using the *Kif7* -/- murine model, we show that the *Kif7* deletion is responsible for a large range of developmental defects in the cerebral cortex, which include: i) alteration of the inhibitory interneurons migration by a combination of intrinsic and extrinsic factors, ii) abnormal formation of cortical layers by the cortical plate neurons and iii) major pathfinding defects in axonal projections between the cortex and the thalamus. Patients carrying mutations in the *KIF7* gene are classified as ciliopathic patients and display developmental delay, ID and epilepsy. These clinical features could thus be caused by an abnormal distribution of excitatory and inhibitory cortical neurons leading to impaired excitatory/inhibitory balance, and by the development of abnormal connections in the cerebral cortex and with others brains structures. By demonstrating focal heterotopia and abnormal thalamo-cortical connectivity in the murine model, we hope to open a new field of clinical investigations using MRI and tractography to identify such defects in patients carrying mutations in the *KIF7* gene.

MATERIAL AND METHODS

Mice. E14.5 embryos of the swiss (for *in situ* hybridization and RNAscope) and C57/Bl6J (for sonic hedgehog immunostaining) strains were obtained from pregnant females purchased at JanvierLabs (France). Male and female wild type (WT) and *Kif7* -/- animals (E14.5, E16.5 and

P0) expressing TdTomato or not in the MGE-derived cIN (Nkx2.1-Cre;Rosa26-TdTomato) were generated in our animal facility by mating male *Kif7* +/-; Nkx2.1-Cre;Rosa26-TdTomato and female *Kif7* +/- mice to produce embryos and P0. Thirty four pregnant females were used. *Kif7* +/- mice are a generous gift of Pr Chi-Chung Hui (the Provider, SickKids Hospital, Toronto, USA) and Prof Bénédicte Durand (the Transferor, CNRS, Lyon, France). Mice were genotyped as described previously [3]. The day of the vaginal plug was noted E0.5. Experiments have been validated and approved by the Ethical committee Charles Darwin (C2EA-05, authorized project 02241.02) and mice were housed and mated according to European guidelines. Both male and female animals were used in this study. Sex is not considered as a biological variable in embryos.

Immunohistochemistry and imaging. Heads of embryos and P0 animals were fixed by immersion in 0.1% picric acid /4% paraformaldehyde (PAF) in phosphate buffer (PB) for 4 hours and then in 4% PAF in PB overnight. After PBS washes, brains were dissected, included in 3% type VII agarose (Sigma, A0701) and sectionned at 70 µm with a vibratome. Immunostaining was performed on free-floating sections as explain previously (Baudoin et al, 2012). Primary antibodies were goat anti SHH-Nter (1:100, R&D system AF464), goat anti Netrin G1a (NG1a) (1:100, R&D system AF1166), rabbit anti TBR1 (1:1000, Abcam ab31940), rabbit anti TBR2 (1:1000, Abcam ab23345), rabbit anti PAX6 (1:100, clone poly19013, Covance PRB-278P), rabbit anti GSH2 (1:2000, Millipore ABN162), chicken anti MAP2 (1:500, Novus, NB30213), and rat CTIP2 (1:1000, Abcam ab18465). Primary antibodies were incubated in PGT (PBS/gelatine 2g per L/TritonX-100 0.25%) with 0.1% glycine and 0.1% lysine for anti Netrin G1a antibodies and 3% BSA for anti SHH-Nter antibodies. Primary antibodies were revealed by immunofluorescence with the appropriate Alexa dye (Molecular Probes) or Cy3 (Jackson laboratories) conjugated secondary antibodies diluted in PGT (1:400). Bisbenzimide (1/5000 in PBT, Sigma) was used for nuclear counterstaining. Sections were mounted in mowiol/DABCO (25mg/mL) and imaged on a macroscope (MVX10 olympus) or an epifluorescence microscope (LEICA DM6000) using X40 and X63 immersion objectives, or a confocal microscope (Leica TCS SP5) using a x40 objective. Double immunotraning were performed when possible and images were representative of what was observed in more than 4 animals per genotype except for heterotopia. Macroscop images were treated to remove background around sections using wand tool in Adobe Photoshop 7.0 software. On epifluorescence and confocal microscop images, acquisition parameters and levels of intensity in Adobe Photoshop 7.0 software were similar for WT and *Kif7* -/-. Merged images were acquired on the same section except for TBR1 with TBR2 aquired on adjacent sections. The

fluorescence intensity along the depth of the cortex was assessed using the plot profile function of ImageJ under a 500 pixels wide line starting in the ventricle to the surface of the brain.

In situ hybridization. Specific antisense RNA probe for *Shh*, *Gli1* and *CxCl12* genes (gift of Marie-Catherine Tiveron) were used for in situ hybridization analyses. DIG-probes were synthesized with a labeling kit according to the manufacturer's instructions (Roche, France). *In situ* hybridization was performed according to a modification of Tiveron et al [45] (see Supplementary material). Sections were mounted on glass slides, dried, dehydrated in graded ethanol solutions, cleared in xylene and coverslipped with Eukitt.

RNAscope. Embryonic E14.5 heads were cuted in cold Leibovitz medium (Invitrogen) and immersion fixed in cold 4% (w/v) paraformaldehyde (PFA) in 0.12 m phosphate buffer, pH 7.4, overnight. Brains were then cryoprotected in PFA 4% /sucrose 10 %, embedded in gelatin 7.5% /sucrose 10% at 4°C and frozen. Biological samples were kept at -80°C until coronally sectioned at 20 µm with cryostat. RNAscope experiment was performed according manufacturer's instructions (RNAScope® Multiplex Fluorescent V2 Assay, ACDbio) after a pre-treatment to remove gelatin. Two different probes/channels were used (C1 for Shh, C2 for Lhx-6). Probes were diluted according manufacturer's instructions (1 Vol of C2 for 50 vol of C1) and dilution of the fluorophores (Opal 520 and 570) was 1:1500. Sections were mounted in mowiol/DABCO (25mg/mL) and imaged on a confocal microscop (Leica TCS SP5) using an immersion X10 or X63 objectives on 10 µm stacks of images (1 image /µm).

DiI experiments. Tiny crystals of DiI (1,1′-dioctadecyl-3,3,3′3′-tetramethylindocarbocyanine perchlorate) were inserted in the dorsal or lateral cortex of WT and *Kif7* -/-embryonic brains fixed at E14.5 by immersion in 4% PAF. Injected brains were stored in 4% PAF at room temperature in the dark for several weeks to allow DiI diffusion. Before sectioning, brains were included in 3% agar. Coronal sections 60 µm thick were prepared with a vibratome and collected individually in 4% PAF. Sections were imaged with a macroscope (MVX10 Olympus).

Whole brain clearing and imaging. E14 and E16 embryos (WT, n=5; *Kif7* -/-, n=6) were collected in cold L15 medium, perfused transcardially with 4% PAF using a binocular microscope. Brains were dissected and postfixed 3 days in 4% PAF at 4°C, and stored in PB at 4°C until clearing. All buffer solutions were supplemented with 0.01% Sodium Azide (Sigma-Aldrich). Whole brain immunostaining and clearing was performed at RT under gentle shaking according to a modified version of the original protocol [46]. Briefly, perfused brains were dehydrated in graded methanol solutions (Fischer Scientific) (20, 50, 80% in ddH_2O, 2x100%,

1h30 each), bleached overnight in 3% hydrogen peroxide (Sigma-Aldrich) in 100% methanol and rehydrated progressively. After PBS washes, brains were blocked and permeabilized 2 days in PBGT (0.2% gelatin (Merck), 0.5% triton X-100 (Sigma-Aldrich) in PBS). Brains were incubated 3 days at 37°C in primary goat anti Netrin G1a (1:100, R&D system AF1166) and rabbit anti Tbr1 (1:1000, Abcam ab31940) antibodies. After 1 day of PBGT washes, brains were incubated 1 day at 37°C in secondary 647 donkey anti-goat (1:1000, Molecular probes,) and cy3 donkey anti-rabbit (1:1000,Jackson laboratories) antibodies.Immunolabeled brains were washed 1 day in PBS, embedded into 1.5% low-melting agarose (type VII, Sigma) in 1% ultra-pure Tris-acetate-EDTA solution, placed in 5-ml tubes (Eppendorf, 0030119452) and dehydrated 1h in each methanol baths (50%, 80% and 2x100%). Samples were then incubated for 3h in 33% methanol / 66% dichloromethane (DCM, Sigma-Aldrich), washed in 100% DCM (2x30 min) and incubated overnight (without shaking) in dibenzyl ether (DBE). Brains were stored in DBE at RT. Cleared samples were imaged on a light-sheet microscope (LaVision Biotec, x6.3 zoom magnification) equipped with a sCMOS camera (Andor Neo) and Imspector Microscope controller software. Imaris (Bitplane) was used for 3D reconstructions, snapshots and movies.

Brain slices. We dissected brains of E14.5 WT and *Kif7* -/- transgenic Nkx2.1-cre, TdTomato embryos in cold L15 medium, embedded in 3% type VII agarose and sectioned coronally with a manual slicer as explained in Baudoin et al, 2012. Forebrain slices 250 µm thick were transferred in Millicell chambers and cultured for 4 hours in F12/DMEM medium supplemented with CFS 10% in a CO2 incubator (Merck Millipore) prior to pharmacological treatment and recording. Slices were incubated in drug for 2 hours before transfer in culture boxes equipped with a bottom glass coverslip for time-lapse imaging.

Pharmacological treatment. Either recombinant Mouse SHH (C25II), N-terminus (464-SH-025, R&D systems) at 0.5µg/mL final or cyclopamine (C4116, Sigma) at 2.5 µM final were added to the culture medium of slices and renewed after 12 hours. Recombinant SHH was reconstituted at 100 µg/mL in sterile PBS with BSA 0.1%. The stock solution of cyclopamine was 10 mM in DMSO and the culture medium of control experiments contained 1/4000 DMSO (vehicle). Control experiments in culture medium with and without vehicle did not differ and were analyzed together.

Videomicroscopy and image processing. Slices were imaged on an inverted microscope (Leica DMI4000) equipped with a spinning disk (Roper Scientific, USA) and a temperature-controlled chamber. Multi-position acquisition was performed with a Coolsnap HQ camera (Roper

Scientific, USA) to allow the recording of the whole cortex. Images were acquired with a X20 objective (LX20, Fluotar, Leica, Germany) and a 561 nm laser (MAG Biosystems, Arizona). Z-stacks of 30 µm were acquired 50 µm away from the slice surface, with a step size of 2 µm and a time interval of 2 or 5 minutes for at least 21 hours. Acquisitions were controlled using the Metamorph software (Roper Scientific, USA). Cell trajectories were reconstructed on movies by tracking manually the cell rear with MTrakJ (ImageJ plugin, NIH, USA) and were clustered according to their position in cortical layers and to their orientation (see details in Fig. 5). The migration speed of cells and the frequency and duration of pauses were extracted from tracking data using an excel macro.

Study design. WT group was compared to *Kif7* -/- group and to pharmacological treatment groups for brain slice experiments. The experimental unit was a single animal for immunohistochemistry analysis and individual cell for videomicroscopy analysis.

Statistical analysis. All data were obtained from at least three independent experiments and are presented as mean ± SEM (standard error of mean). Statistical analyses were performed with the GraphPad Prism software or R. Statistical significance of the data was evaluated using the unpaired two-tailed *t* test, the Mann–Whitney test, the Chi2 test or the Two-way ANOVA test followed by a post-hoc test. Data distribution was tested for normality using the D'Agostino and Pearson omnibus normality test. Values of $P<0.05$ were considered significant. In figures, levels of significance were expressed by * for $P<0.05$, ** for $P<0.01$, *** for $P<0.001$ and **** for $P<0.0001$.

Data availabitily. The data presented in this study are available from the corresponding author upon request without undue reservation.

Acknowledgements. Marie-Christine Tiveron is acknowledged for the gift of the CXCL12 expression vector. We thank all members of the Métin's Team for constructive discussions. We gratefully acknowledge the Imaging plateform facility of the Fer à Moulin Institute for the use of their microscopes, and the animal facility of the Fer à Moulin Institute for animal care and breeding.

Funding. This work was supported by Institut National de la Santé et de la Recherche Médicale (INSERM), Centre National de la Recherche Scientifique (CNRS), Sorbonne University. Agence Nationale de la Recherche (ANR, grant MIGRACIL to C.M.), Fondation pour la

Recherche sur le Cerveau (grant R11080DD to C.M.), Fondation J. Lejeune (grant R14108DD to C.M.).

Author contributions. CM and JM conceptualized the project and supervised the work. MP, VG, SSL, JP, AM, NR, CM and JM perfomed experiments. MP, SSL, AM, NR, CM and JM analyzed the data. MP, VG, SSL, CM and JM wrote the paper.

We declare no Competing interest.

References

1. Park SM, Jang HJ, Lee JH. Roles of Primary Cilia in the Developing Brain. *Front Cell Neurosci*. 2019;13:218. doi:10.3389/fncel.2019.00218

2. Haycraft CJ, Banizs B, Aydin-Son Y, Zhang Q, Michaud EJ, Yoder BK. Gli2 and Gli3 Localize to Cilia and Require the Intraflagellar Transport Protein Polaris for Processing and Function. Barsh G, ed. *PLoS Genet*. 2005;1(4):e53. doi:10.1371/journal.pgen.0010053

3. Cheung HO, Zhang X, Ribeiro A, et al. The kinesin protein Kif7 is a critical regulator of Gli transcription factors in mammalian hedgehog signaling. *Science signaling*. 2009;2(76):ra29. doi:10.1126/scisignal.2000405

4. Endoh-Yamagami S, Evangelista M, Wilson D, et al. The mammalian Cos2 homolog Kif7 plays an essential role in modulating Hh signal transduction during development. *Current biology : CB*. 2009;19(15):1320-1326. doi:10.1016/j.cub.2009.06.046

5. Liem KF, He M, Ocbina PJR, Anderson KV. Mouse Kif7/Costal2 is a cilia-associated protein that regulates Sonic hedgehog signaling. *Proc Natl Acad Sci USA*. 2009;106(32):13377-13382. doi:10.1073/pnas.0906944106

6. Ingham PW, McMahon AP. Hedgehog Signalling: Kif7 Is Not That Fishy After All. *Current Biology*. 2009;19(17):R729-R731. doi:10.1016/j.cub.2009.07.060

7. Pedersen LB, Akhmanova A. Kif7 keeps cilia tips in shape. *Nature cell biology*. 2014;16(7):623-625. doi:10.1038/ncb2997

8. Han Y, Wang B, Cho YS, et al. Phosphorylation of Ci/Gli by Fused Family Kinases Promotes Hedgehog Signaling. *Developmental Cell*. 2019;50(5):610-626.e4. doi:10.1016/j.devcel.2019.06.008

9. al-Gazali LI, Bakalinova D. Autosomal recessive syndrome of macrocephaly, multiple epiphyseal dysplasia and distinctive facial appearance. *Clinical dysmorphology*. 1998;7(3):177-184. doi:10.1097/00019605-199807000-00004

10. Ali BR, Silhavy JL, Akawi NA, Gleeson JG, Al-Gazali L. A mutation in KIF7 is responsible for the autosomal recessive syndrome of macrocephaly, multiple epiphyseal dysplasia and distinctive facial appearance. *Orphanet journal of rare diseases*. 2012;7:27. doi:10.1186/1750-1172-7-27

11. Asadollahi R, Strauss JE, Zenker M, et al. Clinical and experimental evidence suggest a link between KIF7 and C5orf42-related ciliopathies through Sonic Hedgehog signaling. *European journal of human genetics : EJHG*. 2018;26(2):197-209. doi:10.1038/s41431-017-0019-9

12. Barakeh D, Faqeih E, Anazi S, et al. The many faces of KIF7. *Human genome variation*. 2015;2:15006. doi:10.1038/hgv.2015.6

13. Ibisler A, Hehr U, Barth A, Koch M, Epplen JT, Hoffjan S. Novel KIF7 Mutation in a Tunisian Boy with Acrocallosal Syndrome: Case Report and Review of the Literature. *Molecular syndromology*. 2015;6(4):173-180. doi:10.1159/000439414

14. Niceta M, Dentici ML, Ciolfi A, et al. Co-occurrence of mutations in KIF7 and KIAA0556 in Joubert syndrome with ocular coloboma, pituitary malformation and growth hormone deficiency: a case report and literature review. *BMC pediatrics*. 2020;20(1):120. doi:10.1186/s12887-020-2019-0

15. Putoux A, Baas D, Paschaki M, et al. Altered GLI3 and FGF8 signaling underlies acrocallosal syndrome phenotypes in Kif7 depleted mice. *Human molecular genetics*. 2019;28(6):877-887. doi:10.1093/hmg/ddy392

16. Putoux A, Nampoothiri S, Laurent N, et al. Novel KIF7 mutations extend the phenotypic spectrum of acrocallosal syndrome. *Journal of medical genetics*. 2012;49(11):713-720. doi:10.1136/jmedgenet-2012-101016

17. Tunovic S, Baranano KW, Barkovich JA, Strober JB, Jamal L, Slavotinek AM. Novel KIF7 missense substitutions in two patients presenting with multiple malformations and features of acrocallosal syndrome. *American journal of medical genetics Part A*. 2015;167A(11):2767-2776. doi:10.1002/ajmg.a.37249

18. Walsh DM, Shalev SA, Simpson MA, et al. Acrocallosal syndrome: identification of a novel KIF7 mutation and evidence for oligogenic inheritance. *European journal of medical genetics*. 2013;56(1):39-42. doi:10.1016/j.ejmg.2012.10.004

19. Dafinger C, Liebau MC, Elsayed SM, et al. Mutations in KIF7 link Joubert syndrome with Sonic Hedgehog signaling and microtubule dynamics. *The Journal of clinical investigation*. 2011;121(7):2662-2667. doi:10.1172/JCI43639

20. Chiang C, Litingtung Y, Lee E, et al. Cyclopia and defective axial patterning in mice lacking Sonic hedgehog gene function. *Nature*. 1996;383(6599):407-413. doi:10.1038/383407a0

21. Shimamura K, Rubenstein JLR. Inductive interactions direct early regionalization of the mouse forebrain. *Development*. 1997;124(14):2709-2718. doi:10.1242/dev.124.14.2709

22. Kohtz JD, Baker DP, Corte G, Fishell G. Regionalization within the mammalian telencephalon is mediated by changes in responsiveness to Sonic Hedgehog. *Development*. 1998;125(24):5079-5089. doi:10.1242/dev.125.24.5079

23. Machold R, Hayashi S, Rutlin M, et al. Sonic Hedgehog Is Required for Progenitor Cell Maintenance in Telencephalic Stem Cell Niches. *Neuron*. 2003;39(6):937-950. doi:10.1016/S0896-6273(03)00561-0

24. Xu Q, Wonders CP, Anderson SA. Sonic hedgehog maintains the identity of cortical interneuron progenitors in the ventral telencephalon. *Development*. 2005;132(22):4987-4998. doi:10.1242/dev.02090

25. Xu Q, Guo L, Moore H, Waclaw RR, Campbell K, Anderson SA. Sonic Hedgehog Signaling Confers Ventral Telencephalic Progenitors with Distinct Cortical Interneuron Fates. *Neuron*. 2010;65(3):328-340. doi:10.1016/j.neuron.2010.01.004

26. Sousa VH, Fishell G. Sonic hedgehog functions through dynamic changes in temporal competence in the developing forebrain. *Current Opinion in Genetics & Development*. 2010;20(4):391-399. doi:10.1016/j.gde.2010.04.008

27. Komada M, Saitsu H, Kinboshi M, Miura T, Shiota K, Ishibashi M. Hedgehog signaling is involved in development of the neocortex. *Development*. 2008;135(16):2717-2727. doi:10.1242/dev.015891

28. Dahmane N, Sánchez P, Gitton Y, et al. The Sonic Hedgehog-Gli pathway regulates dorsal brain growth and tumorigenesis. *Development*. 2001;128(24):5201-5212. doi:10.1242/dev.128.24.5201

29. Baudoin JP, Viou L, Launay PS, et al. Tangentially migrating neurons assemble a primary cilium that promotes their reorientation to the cortical plate. *Neuron*. 2012;76(6):1108-1122. doi:10.1016/j.neuron.2012.10.027

30. Higginbotham H, Eom TY, Mariani LE, et al. Arl13b in primary cilia regulates the migration and placement of interneurons in the developing cerebral cortex. *Developmental cell*. 2012;23(5):925-938. doi:10.1016/j.devcel.2012.09.019

31. Komada M. Sonic hedgehog signaling coordinates the proliferation and differentiation of neural stem/progenitor cells by regulating cell cycle kinetics during development of the neocortex. *Congenital anomalies*. 2012;52(2):72-77. doi:10.1111/j.1741-4520.2012.00368.x

32. Komada M, Iguchi T, Takeda T, Ishibashi M, Sato M. Smoothened controls cyclin D2 expression and regulates the generation of intermediate progenitors in the developing cortex. *Neuroscience letters*. 2013;547:87-91. doi:10.1016/j.neulet.2013.05.006

33. Hasenpusch-Theil K, Theil T. The Multifaceted Roles of Primary Cilia in the Development of the Cerebral Cortex. *Frontiers in cell and developmental biology*. 2021;9:630161. doi:10.3389/fcell.2021.630161

34. Hui CC, Slusarski D, Platt KA, Holmgren R, Joyner AL. Expression of Three Mouse Homologs of the Drosophila Segment Polarity Gene cubitus interruptus, Gli, Gli-2, and Gli-3, in Ectoderm- and Mesoderm-Derived Tissues Suggests Multiple Roles during Postimplantation Development. *Developmental Biology*. 1994;162(2):402-413. doi:10.1006/dbio.1994.1097

35. Yu W, Wang Y, McDonnell K, Stephen D, Bai CB. Patterning of ventral telencephalon requires positive function of Gli transcription factors. *Developmental Biology*. 2009;334(1):264-275. doi:10.1016/j.ydbio.2009.07.026

36. Park HL, Bai C, Platt KA, et al. Mouse *Gli1* mutants are viable but have defects in SHH signaling in combination with a *Gli2* mutation. *Development*. 2000;127(8):1593-1605. doi:10.1242/dev.127.8.1593

37. Bai CB, Joyner AL. *Gli1* can rescue the in vivo function of *Gli2*. *Development*. 2001;128(24):5161-5172. doi:10.1242/dev.128.24.5161

38. Ding Q, Motoyama J, Gasca S, et al. Diminished Sonic hedgehog signaling and lack of floor plate differentiation in *Gli2* mutant mice. *Development*. 1998;125(14):2533-2543. doi:10.1242/dev.125.14.2533

39. Tole S, Ragsdale CW, Grove EA. Dorsoventral Patterning of the Telencephalon Is Disrupted in the Mouse Mutant extra-toesJ. *Developmental Biology*. 2000;217(2):254-265. doi:10.1006/dbio.1999.9509

40. Rallu M, Machold R, Gaiano N, Corbin JG, McMahon AP, Fishell G. Dorsoventral patterning is established in the telencephalon of mutants lacking both Gli3 and Hedgehog signaling. *Development*. 2002;129(21):4963-4974. doi:10.1242/dev.129.21.4963

41. Wang H, Ge G, Uchida Y, Luu B, Ahn S. *Gli3* Is Required for Maintenance and Fate Specification of Cortical Progenitors. *J Neurosci*. 2011;31(17):6440-6448. doi:10.1523/JNEUROSCI.4892-10.2011

42. Wilson SL, Wilson JP, Wang C, Wang B, McConnell SK. Primary cilia and Gli3 activity regulate cerebral cortical size. *Developmental Neurobiology*. 2012;72(9):1196-1212. doi:10.1002/dneu.20985

43. Putoux A, Baas D, Paschaki M, et al. Altered GLI3 and FGF8 signaling underlies acrocallosal syndrome phenotypes in Kif7 depleted mice. *Human molecular genetics*. 2019;28(6):877-887. doi:10.1093/hmg/ddy392

44. Guo J, Higginbotham H, Li J, et al. Developmental disruptions underlying brain abnormalities in ciliopathies. *Nature communications*. 2015;6:7857. doi:10.1038/ncomms8857

45. Tiveron MC, Hirsch MR, Brunet JF. The Expression Pattern of the Transcription Factor Phox2 Delineates Synaptic Pathways of the Autonomic Nervous System. *J Neurosci*. 1996;16(23):7649-7660. doi:10.1523/JNEUROSCI.16-23-07649.1996

46. Renier N, Adams EL, Kirst C, et al. Mapping of Brain Activity by Automated Volume Analysis of Immediate Early Genes. *Cell*. 2016;165(7):1789-1802. doi:10.1016/j.cell.2016.05.007

47. Maurya AK, Ben J, Zhao Z, et al. Positive and negative regulation of Gli activity by Kif7 in the zebrafish embryo. *PLoS genetics*. 2013;9(12):e1003955. doi:10.1371/journal.pgen.1003955

48. Klejnot M, Kozielski F. Structural insights into human Kif7, a kinesin involved in Hedgehog signalling. *Acta crystallographica Section D, Biological crystallography*. 2012;68(Pt 2):154-159. doi:10.1107/S0907444911053042

49. Putoux A, Thomas S, Coene KL, et al. KIF7 mutations cause fetal hydrolethalus and acrocallosal syndromes. *Nature genetics*. 2011;43(6):601-606. doi:10.1038/ng.826

50. Chen J, Laclef C, Moncayo A, et al. The ciliopathy gene Rpgrip1l is essential for hair follicle development. *The Journal of investigative dermatology*. 2015;135(3):701-709. doi:10.1038/jid.2014.483

51. Walczak-Sztulpa J, Eggenschwiler J, Osborn D, et al. Cranioectodermal Dysplasia, Sensenbrenner syndrome, is a ciliopathy caused by mutations in the IFT122 gene. *American journal of human genetics*. 2010;86(6):949-956. doi:10.1016/j.ajhg.2010.04.012

52. Fotaki V, Yu T, Zaki PA, Mason JO, Price DJ. Abnormal positioning of diencephalic cell types in neocortical tissue in the dorsal telencephalon of mice lacking functional Gli3. *The Journal of neuroscience : the official journal of the Society for Neuroscience*. 2006;26(36):9282-9292. doi:10.1523/JNEUROSCI.2673-06.2006

53. Magnani D, Hasenpusch-Theil K, Jacobs EC, Campagnoni AT, Price DJ, Theil T. The Gli3 hypomorphic mutation Pdn causes selective impairment in the growth, patterning, and axon guidance capability of the lateral ganglionic eminence. *The Journal of neuroscience : the official journal of the Society for Neuroscience*. 2010;30(41):13883-13894. doi:10.1523/JNEUROSCI.3650-10.2010

54. Price DJ, Kennedy H, Dehay C, et al. The development of cortical connections. *The European journal of neuroscience*. 2006;23(4):910-920. doi:10.1111/j.1460-9568.2006.04620.x

55. Hatanaka Y, Yamauchi K. Excitatory Cortical Neurons with Multipolar Shape Establish Neuronal Polarity by Forming a Tangentially Oriented Axon in the Intermediate Zone. *Cerebral Cortex*. 2013;23(1):105-113. doi:10.1093/cercor/bhr383

56. Kon E, Cossard A, Jossin Y. Neuronal Polarity in the Embryonic Mammalian Cerebral Cortex. *Front Cell Neurosci*. 2017;11:163. doi:10.3389/fncel.2017.00163

57. Braisted JE, Catalano SM, Stimac R, et al. Netrin-1 Promotes Thalamic Axon Growth and Is Required for Proper Development of the Thalamocortical Projection. *J Neurosci*. 2000;20(15):5792-5801. doi:10.1523/JNEUROSCI.20-15-05792.2000

58. Métin C, Godement P. The Ganglionic Eminence May Be an Intermediate Target for Corticofugal and Thalamocortical Axons. *J Neurosci*. 1996;16(10):3219-3235. doi:10.1523/JNEUROSCI.16-10-03219.1996

59. Denaxa M, Chan CH, Schachner M, Parnavelas JG, Karagogeos D. The adhesion molecule TAG-1 mediates the migration of cortical interneurons from the ganglionic eminence along the corticofugal fiber system. *Development*. 2001;128(22):4635-4644. doi:10.1242/dev.128.22.4635

60. Tanaka D, Nakaya Y, Yanagawa Y, Obata K, Murakami F. Multimodal tangential migration of neocortical GABAergic neurons independent of GPI-anchored proteins. *Development*. 2003;130(23):5803-5813. doi:10.1242/dev.00825

61. Yokota Y, Ghashghaei HT, Han C, Watson H, Campbell KJ, Anton ES. Radial Glial Dependent and Independent Dynamics of Interneuronal Migration in the Developing Cerebral Cortex. Chan-Ling T, ed. *PLoS ONE*. 2007;2(8):e794. doi:10.1371/journal.pone.0000794

62. Tiveron MC, Rossel M, Moepps B, et al. Molecular interaction between projection neuron precursors and invading interneurons via stromal-derived factor 1 (CXCL12)/CXCR4 signaling in the cortical subventricular zone/intermediate zone. *The Journal of neuroscience : the official journal of the Society for Neuroscience*. 2006;26(51):13273-13278. doi:10.1523/JNEUROSCI.4162-06.2006

63. Stumm RK, Zhou C, Ara T, et al. CXCR4 Regulates Interneuron Migration in the Developing Neocortex. *J Neurosci*. 2003;23(12):5123-5130. doi:10.1523/JNEUROSCI.23-12-05123.2003

64. Li G, Adesnik H, Li J, et al. Regional Distribution of Cortical Interneurons and Development of Inhibitory Tone Are Regulated by Cxcl12/Cxcr4 Signaling. *J Neurosci*. 2008;28(5):1085-1098. doi:10.1523/JNEUROSCI.4602-07.2008

65. Atkins M, Wurmser M, Darmon M, Roche F, Nicol X, Métin C. CXCL12 targets the primary cilium cAMP/cGMP ratio to regulate cell polarity during migration. *Nat Commun*. 2023;14(1):8003. doi:10.1038/s41467-023-43645-w

66. Bellion A. Nucleokinesis in Tangentially Migrating Neurons Comprises Two Alternating Phases: Forward Migration of the Golgi/Centrosome Associated with Centrosome Splitting and Myosin Contraction at the Rear. *Journal of Neuroscience*. 2005;25(24):5691-5699. doi:10.1523/JNEUROSCI.1030-05.2005

67. Sahara S, Kawakami Y, Izpisua Belmonte JC, O'Leary DD. Sp8 exhibits reciprocal induction with Fgf8 but has an opposing effect on anterior-posterior cortical area patterning. *Neural development*. 2007;2:10. doi:10.1186/1749-8104-2-10

68. Nery S, Wichterle H, Fishell G. Sonic hedgehog contributes to oligodendrocyte specification in the mammalian forebrain. *Development*. 2001;128(4):527-540. doi:10.1242/dev.128.4.527

69. Lee J, Ekker S, von Kessler D, Porter J, Sun B, Beachy P. Autoproteolysis in hedgehog protein biogenesis. *Science*. 1994;266(5190):1528-1537. doi:10.1126/science.7985023

70. Loulier K, Ruat M, Traiffort E. Analysis of hedgehog interacting protein in the brain and its expression in nitric oxide synthase-positive cells. *Neuroreport*. 2005;16(17):1959-1962. doi:10.1097/01.wnr.0000187632.91375.81

71. Kiecker C, Lumsden A. Hedgehog signaling from the ZLI regulates diencephalic regional identity. *Nat Neurosci*. 2004;7(11):1242-1249. doi:10.1038/nn1338

72. Magnani D, Hasenpusch-Theil K, Benadiba C, et al. Gli3 controls corpus callosum formation by positioning midline guideposts during telencephalic patterning. *Cereb Cortex*. 2014;24(1):186-198. doi:10.1093/cercor/bhs303

73. Marín O. Interneuron dysfunction in psychiatric disorders. *Nat Rev Neurosci*. 2012;13(2):107-120. doi:10.1038/nrn3155

74. Barkovich AJ, Dobyns WB, Guerrini R. Malformations of Cortical Development and Epilepsy. *Cold Spring Harbor Perspectives in Medicine*. 2015;5(5):a022392-a022392. doi:10.1101/cshperspect.a022392

75. Yue Y, Engelke MF, Blasius TL, Verhey KJ. Hedgehog-induced ciliary trafficking of kinesin-4 motor KIF7 requires intraflagellar transport but not KIF7's microtubule binding. *Molecular biology of the cell*. 2022;33(1):br1. doi:10.1091/mbc.E21-04-0215

76. Vilboux T, Malicdan MC, Roney JC, et al. CELSR2, encoding a planar cell polarity protein, is a putative gene in Joubert syndrome with cortical heterotopia, microophthalmia, and growth hormone deficiency. *American journal of medical genetics Part A*. 2017;173(3):661-666. doi:10.1002/ajmg.a.38005

77. Boutin C, Goffinet AM, Tissir F. Celsr1–3 Cadherins in PCP and Brain Development. In: *Current Topics in Developmental Biology*. Vol 101. Elsevier; 2012:161-183. doi:10.1016/B978-0-12-394592-1.00010-7

78. Hakanen J, Parmentier N, Sommacal L, et al. The Celsr3-Kif2a axis directs neuronal migration in the postnatal brain. *Progress in Neurobiology*. 2022;208:102177. doi:10.1016/j.pneurobio.2021.102177

79. Alcauter S, Lin W, Smith JK, et al. Development of thalamocortical connectivity during infancy and its cognitive correlations. *The Journal of neuroscience : the official journal of the Society for Neuroscience*. 2014;34(27):9067-9075. doi:10.1523/JNEUROSCI.0796-14.2014

80. Jakab A, Natalucci G, Koller B, Tuura R, Ruegger C, Hagmann C. Mental development is associated with cortical connectivity of the ventral and nonspecific thalamus of preterm newborns. *Brain and behavior*. 2020;10(10):e01786. doi:10.1002/brb3.1786

81. Tissir F, Bar I, Jossin Y, De Backer O, Goffinet AM. Protocadherin Celsr3 is crucial in axonal tract development. *Nature neuroscience*. 2005;8(4):451-457. doi:10.1038/nn1428

82. Wang Y, Thekdi N, Smallwood PM, Macke JP, Nathans J. Frizzled-3 is required for the development of major fiber tracts in the rostral CNS. *The Journal of neuroscience : the official journal of the Society for Neuroscience*. 2002;22(19):8563-8573. doi:10.1523/JNEUROSCI.22-19-08563.2002

83. Moreau MX, Saillour Y, Cwetsch AW, Pierani A, Causeret F. Single-cell transcriptomics of the early developing mouse cerebral cortex disentangle the spatial and temporal components of neuronal fate acquisition. *Development*. 2021;148(14):dev197962. doi:10.1242/dev.197962

84. Huang X, Liu J, Ketova T, et al. Transventricular delivery of Sonic hedgehog is essential to cerebellar ventricular zone development. *Proc Natl Acad Sci USA*. 2010;107(18):8422-8427. doi:10.1073/pnas.0911838107

85. Zakaria M, Ferent J, Hristovska I, et al. The Shh receptor Boc is important for myelin formation and repair. *Development*. 2019;146(9). doi:10.1242/dev.172502

86. He M, Subramanian R, Bangs F, et al. The kinesin-4 protein Kif7 regulates mammalian Hedgehog signalling by organizing the cilium tip compartment. *Nature cell biology*. 2014;16(7):663-672. doi:10.1038/ncb2988

87. Vyas N, Walvekar A, Tate D, et al. Vertebrate Hedgehog is secreted on two types of extracellular vesicles with different signaling properties. *Sci Rep*. 2014;4(1):7357. doi:10.1038/srep07357

88. Eitan E, Petralia RS, Wang YX, Indig FE, Mattson MP, Yao PJ. Probing extracellular Sonic hedgehog in neurons. *Biology open*. 2016;5(8):1086-1092. doi:10.1242/bio.019422

89. Hasenpusch-Theil K, Laclef C, Colligan M, et al. A transient role of the ciliary gene Inpp5e in controlling direct versus indirect neurogenesis in cortical development. *eLife*. 2020;9. doi:10.7554/eLife.58162

90. Higginbotham H, Guo J, Yokota Y, et al. Arl13b-regulated cilia activities are essential for polarized radial glial scaffold formation. *Nature neuroscience*. 2013;16(8):1000-1007. doi:10.1038/nn.3451

91. Lysko DE, Putt M, Golden JA. SDF1 regulates leading process branching and speed of migrating interneurons. *The Journal of neuroscience : the official journal of the Society for Neuroscience*. 2011;31(5):1739-1745. doi:10.1523/JNEUROSCI.3118-10.2011

Figures and Legends to figure

Mutation	Domain lacking, truncated or mutation	Brain		Ref
		Clinical feature	Anatomical defects (cortical in bold)	
Hom c.67C>T, p.Arg33*	No kinesin motor and no Gli binding	DD/ID	Wide ventricles - Macrocephaly CC agenesis/hypoplasia - MTS	1
Hom c.233_234del, p.Leu78Profs*2	Truncated kinesin motor and no Gli binding	DD/ID	Macrocephaly- CC agenesis- MTS	1
Hom c.587dupT, p.Glu197Glyfs*19	Truncated kinesin motor, no Gli binding	DD/ID	Macrocephaly - CC agenesis	1
Hom c.687delG, p.Arg230Alafs*92	Truncated kinesin motor, no Gli binding	DD/ID	Wide ventricles – Macrocephaly - CC agenesis - **Poor frontal cortical development**	1
Hom c.217 delG, p.Ala73Profs*109	No Gli binding	DD/ID	CC agenesis/hypoplasia - MTS	2
Hom c.653_662del, p.218-221del	Deletion in kinesin motor	DD/ID	Wide ventricles – Macrocephaly - CC agenesis - **Cortical atrophy**	3
Hom c.1639_1640delinsT, p.Gly547Serfs*5	No Coiled-coil	DD/ID	Macrocephaly- MTS - CC agenesis/hypoplasia - **Temporal pachygyria**	1
Hom c.1643dupC, p.Arg549Alafs*40	No coiled-coil	DD/Mild ID	Macrocephaly - CC dysgenesis - Cerebellar hypotrophy	4
Hom c.1643dupC, p.Arg549Alafs*40	No coiled-coil	DD/Mild ID	Macrocephaly - CC agenesis - MTS	4
Hom c.2164G>T, p.Glu722*	No coiled-coil	DD/Mild ID	Macrocephaly	4
Hom c.2335G>T, p.Glu779 *	No Coiled-coil	DD/ID - Seizure	Macrocephaly - CC agenesis - Cerebellar hypoplasia - Abnormal formation of the brainstem	5
Hom c.2896_2897del	Deletion in Coiled-coil	DD/ID	CC dysgenesis	6
Hom c.3001C>T, p.Gln1001*	Truncated Coiled-coil	DD/ID	Wide ventricles – Macrocephaly - CC agenesis/hypoplasia- MTS	1
Hom c.529+2T>C	Mutation in kinesin motor	DD	MTS	7
c.2593-3C>G //c.3001C>T, p.Gln1001*	Mutation in Coiled-coil //Truncated Coiled-coil	ID	Macrocephaly - CC hypoplasia - MTS	7
c.1019dupT, p.Asn341Glnfs*122 // c.3331C>T, p.Arg1111*	Truncated kinesin motor and no Gli binding //Truncated Coiled-coil	DD	CC agenesis	7
Hom c2593 C>G //c3001C>T, p.? // p.Gln1001*	Mutation in Coiled-coil //Truncated Coiled-coil	DD/ID- Seizure	Macrocephaly - CC agenesis	4
Hom c.2272G>T	Mutation in Coiled-coil	DD/ID - Seizure	CC agenesis	6
Hom c.3179A >G	Mutation in Coiled-coil	DD/ Very mild ID	Macrocephaly – MTS - CC agenesis/hypoplasia - **Temporo-parietal atrophy**	8,9
c.461G>A // c.2959 G>A	Mutation in Coiled-coil	DD/ID - Seizure	Hydrocephalus - Cerebellar hypoplasia - CC agenesis/hypoplasia - **Pachygyria - Heterotopia**	10
c.3365C>G // c.2482G>A	Mutation in Coiled-coil	DD/ID - Seizure – Ataxia	CC agenesis/hypoplasia	10
Hom c2593-3 C>G	Mutation in Coiled-coil	DD/Mild ID	Macrocephaly - CC hypoplasy Large asymmetrical cisterna magna	4
Hom c.3331C>T	Mutation in Coiled-coil	DD/ID	CC agenesis - MTS	6

Table 1. **Clinical diagnosis of patients carrying mutation in the *KIF7* gene on both alleles from the literature.** The ablated or mutated domains were identified. Clinical features associated with cortical dysfunction are listed. Among cerebral defects, those observed in the cortex are enlighted. DD, developmental delay; ID, intellectual deficit; CC, corpus callosum; MTS, molar tooth sign.

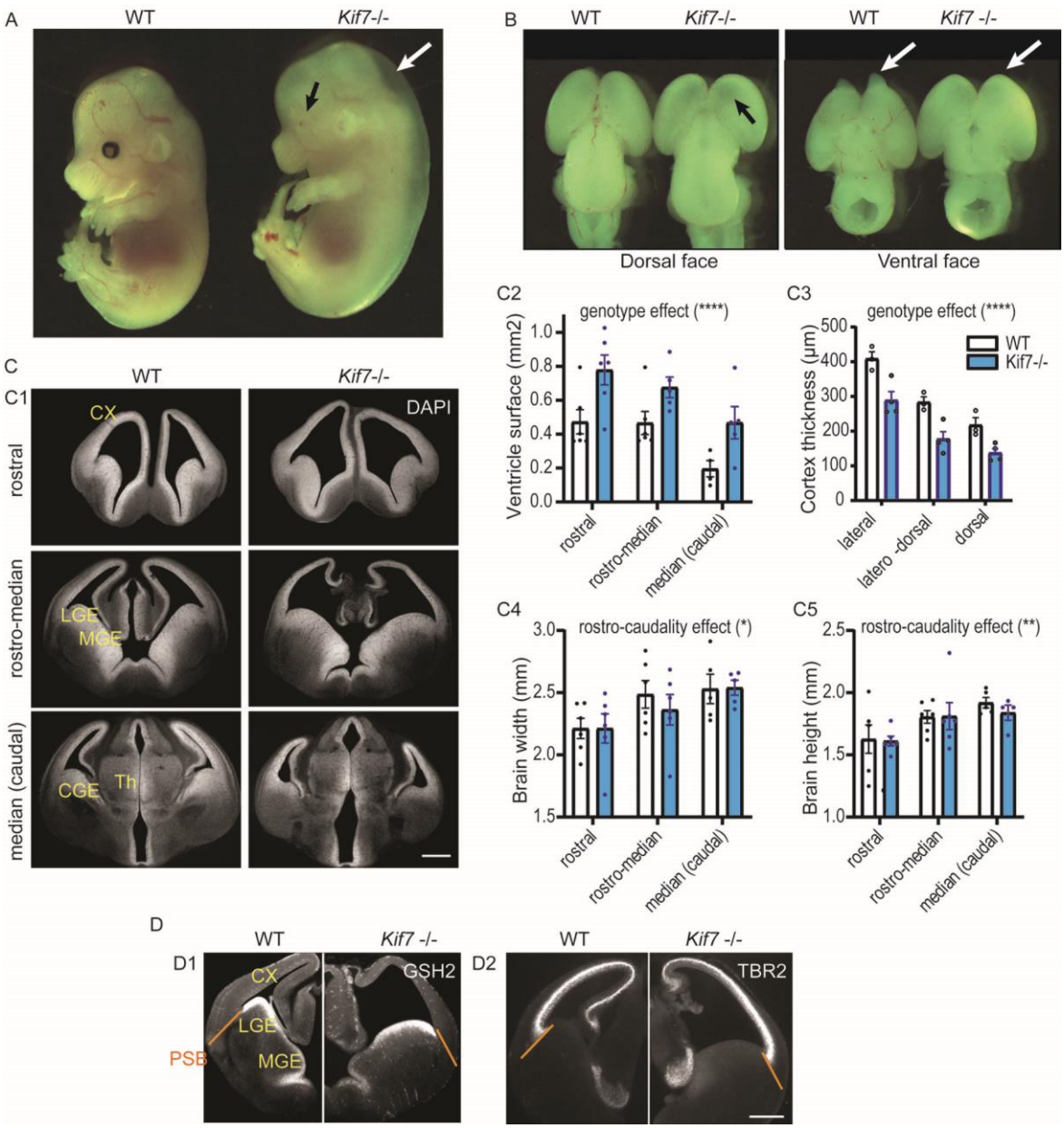

Figure 1. *Kif7* deletion alters cortical anatomy at E14.5 but preserves the dorso-ventral patterning of the telencephalon. **(A)** *Kif7* -/- embryos are microphtalmic (black arrow) and exhibit skin laxity (white arrow). **(B)** External examination of the brain reveals the thinning of the dorsal telencephalon (black arrow, left panel) and the lack of olfactory bulbs (white arrows, right panel). **(C)** DAPI staining of rostro-caudal series of coronal sections (C1) illustrates the anatomical defects of *Kif7* -/- embryonic brains that are quantified in C2-C5. The ventricles of *Kif7* -/- embryos are strongly enlarged (C2), their cortical thickness strongly decreased (C3), resulting in minimal brain width (C4) and height (C5) changes. Statistical significance was tested by Two-way ANOVA or mixed model (GraphPad 8.1.0). In C2 (WT, n=4-6, *Kif7* -/-; n=5-6 depending on the rostro-caudal level), C3 (WT, n=3; *Kif7* -/-, n= 4), mix model reveals a genotype effect ($p<0.0001$). No genotype effect was observed in C4 (WT, n=5-6; n=5-6 for

Kif7 -/- depending on the rostro-caudal level), C5 (WT, n=5-6; *Kif7* -/-, n=4-6 depending on the rostro-caudal level), but a significant effect of the rostro-caudal level on brain width (C4, *P*=0.0441) and height (C5, *P*=0.092). **D.** The pallium-subpallium boundary (PSB) identified by the limit of expression of ventral (GSH2, left panels) and dorsal (TBR2, right panels) telencephalic markers remains well-defined in *Kif7* -/- embryos. Graphs in C2-C5 represent the means and S.E.M. PSB, pallium-subpallium boundary; CX, cortex; LGE, lateral ganglionic eminence; MGE, median ganglionic eminence; CGE, lateral ganglionic eminence; Th, thalamus. Scale bars, 250 µm.

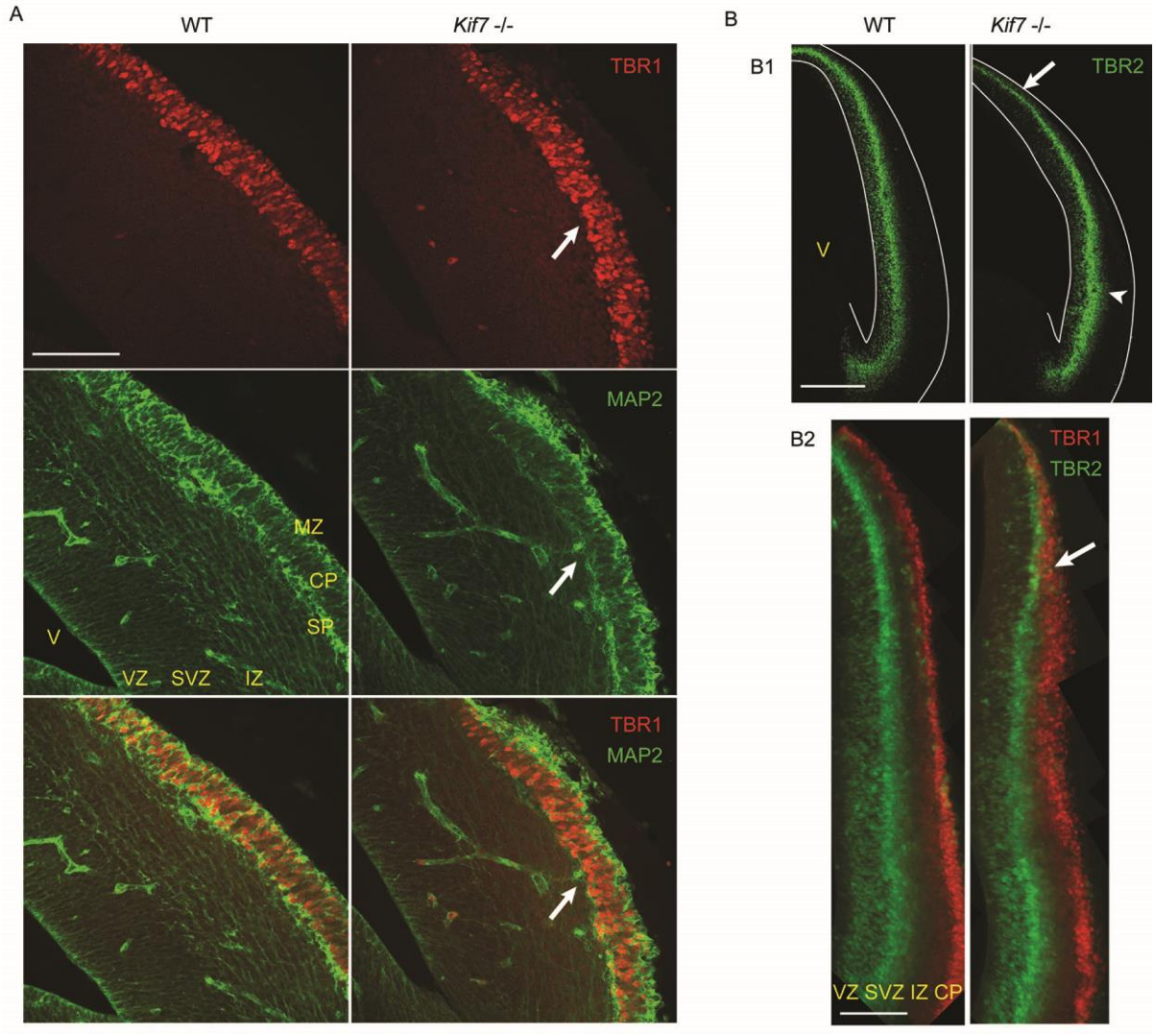

Figure 2. Histological alterations in the developing cortex of E14.5 *Kif7* -/- embryos. Coronal sections representative of E14.5 wild type (WT) and E14.5 *Kif7* -/- embryos imaged on confocal (A) or epifluorescence (B1) microscopes, and on a macroscope (B2). **(A)** The TBR1(+) staining (red) of the cortical plate is more clustered in *Kif7* -/- than in WT embryos, and the MAP2(+) staining (green) of the subplate is absent in the dorsal cortex of *Kif7* -/- embryos (white arrow, right column). **(B)** The TBR2(+) layer (green) of secondary progenitors appears disorganized in the lateral cortex of the *Kif7* -/- embryos (white arrowhead in B1). In the dorsal cortex of *Kif7* -/- embryos (white arows in B1, B2), the TBR2(+) cells (green) form a disorganized layer that reaches the brain surface (B1) where it intermingles with TBR1(+) cells (B2, red cells). V, ventricle; VZ, ventricular zone; SVZ, subventricular zone; IZ, intermediate zone; MZ, marginal zone; CP, cortical plate. Scale bars: 100 µm (A), 200 µm (B1, B2).

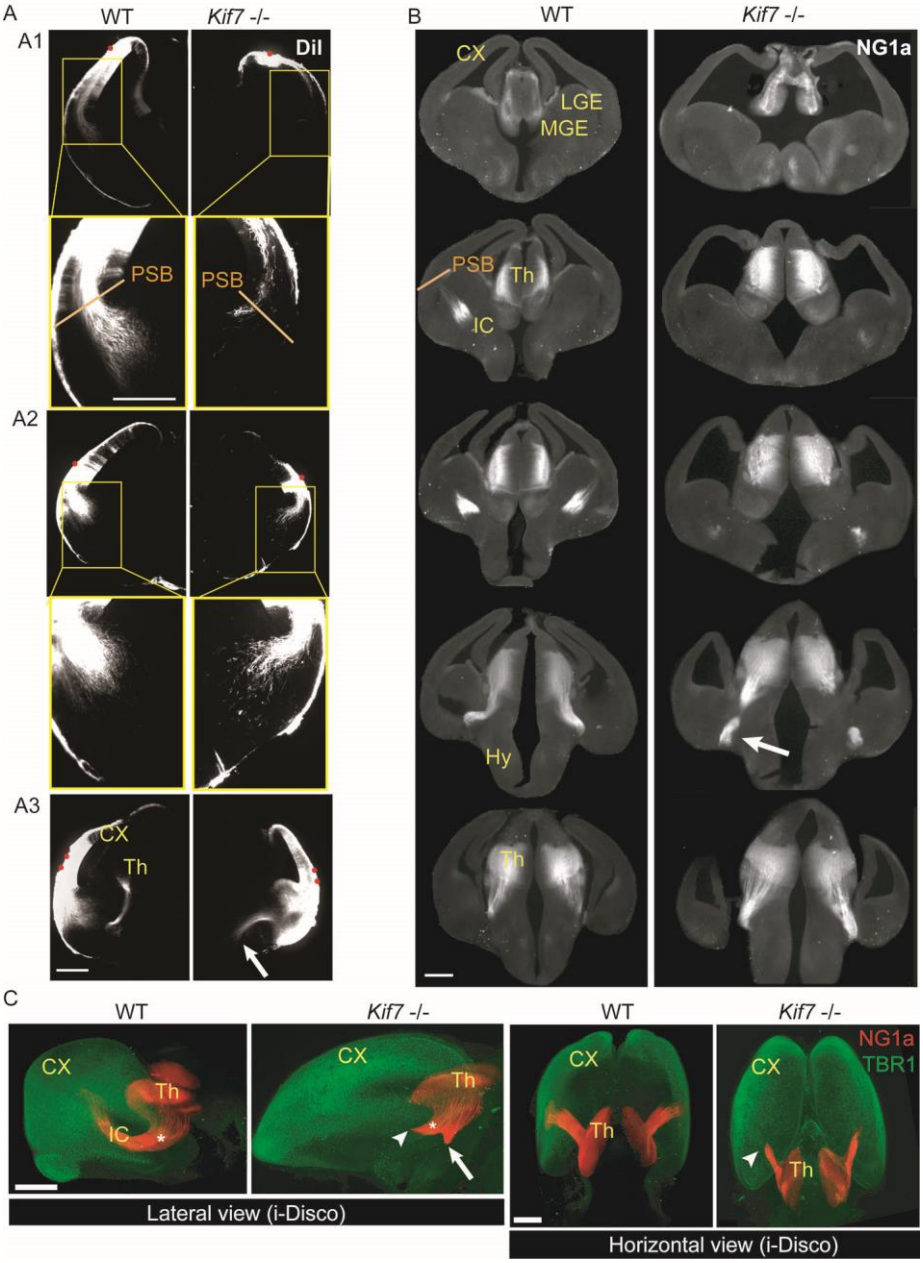

Figure 3. *Kif7* deletion disrupts of the connectivity between the cortex and the thalamus at E14.5. (A) Panels illustrate the corticofugal projection labeled by DiI crystal (red dots) positioned in the dorsal (A1) and lateral (A2,A3) cortex of wild type (WT, left) and *Kif7* -/- (right) embryos on vibratome sections performed 30 days after DiI placement. In *Kif7* -/- embryos, less axons project from the dorsal (A1) and lateral (A2) cortex to the subpallium than in WT. Compare enlarged views of the projections below A1 and A2. Cortical injections in *Kif7* -/- embryos do not label thalamic axons (compare left and right panels in A3) but label a ventral projection (A3, white arrow). **(B)** Rostro-caudal series of coronal sections immunostained with anti-Netrin G1a (NG1a) antibodies compare the trajectory of thalamo-cortical axons (TCA) in a WT (left) and in a *Kif7* -/- (right) embryo. Thalamo-cortical axons reach the pallium-

subpallium boundary (PSB) of the WT embryo whereas they are lost in the ventral forebrain of the mutant (right panel, white arrow). **C.** Representative three-dimensional reconstruction of WT and *Kif7* -/- brains immunostained as a whole with NG1a (red) and TBR1 (green) antibodies before transparization and imaging with a light sheet microscope. Compared to TCA in the WT that form a bundle extending in the internal capsule (IC), TCA in the *Kif7* -/- brain organize two short bundles, one directed to the IC that stops soon after entering the IC, and the other one oriented caudally and ventrally. PSB, pallium-subpallium boundary; CX, cortex; LGE, lateral ganglionic eminence; MGE, median ganglionic eminence; Th, thalamus; Hy, hypothalamus. IC, internal capsule. Scale bars: 250 µm.

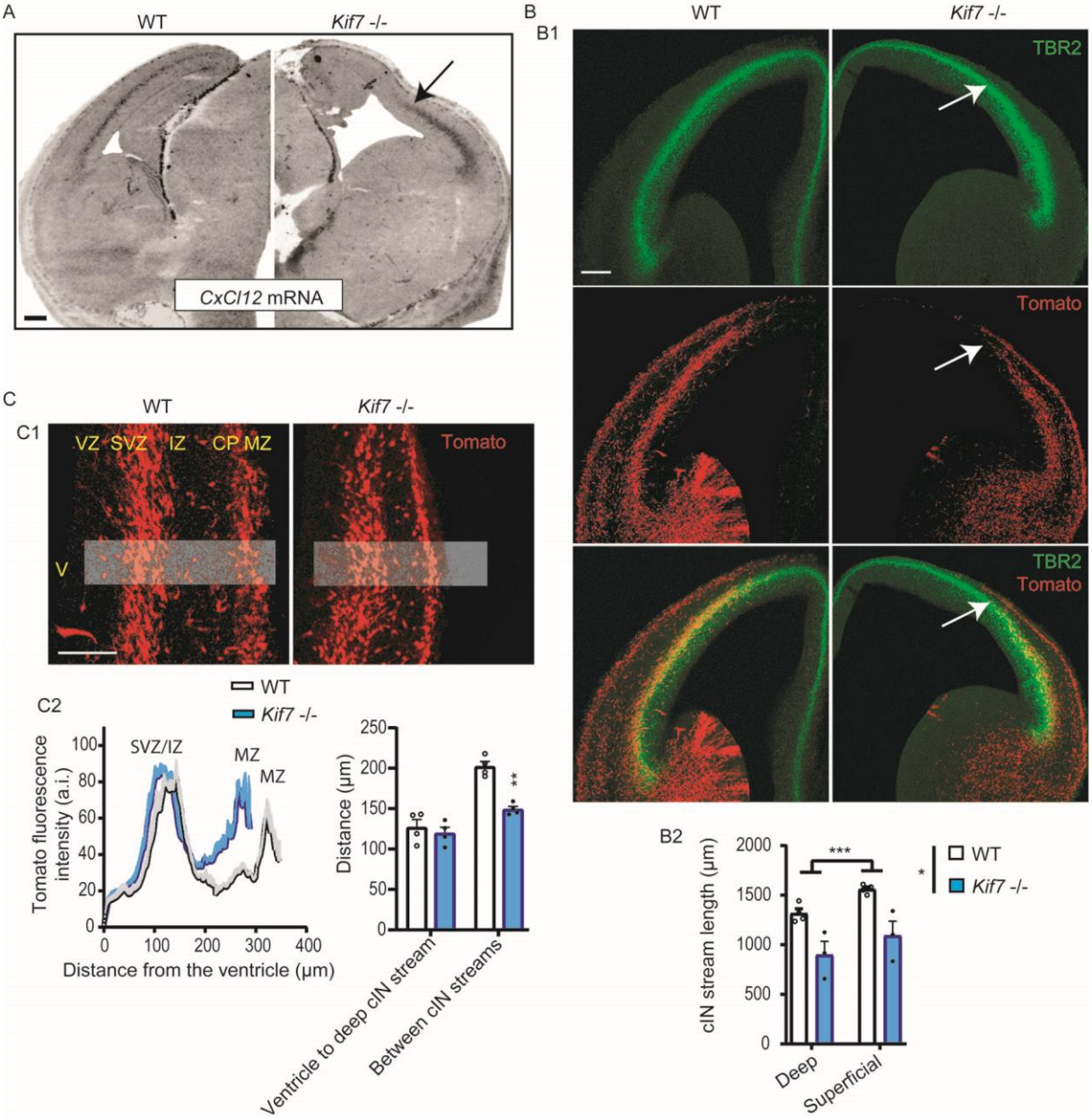

Figure 4. Altered *Cxcl12* transcript expression and abnormal cortical distribution of cIN at E14.5 in *Kif7* -/- brains. (A) Panels compare the distribution of *Cxcl12* mRNA in wild type (WT, left panel) and *Kif7* -/- (right panel) forebrain coronal sections at E14.5. The WT section shows *Cxcl12* transcript enrichment in a deep cortical layer already identified as the SVZ. In the *Kif7* -/- cortical section, the expression of *Cxcl12* transcripts is reduced to the lateral part of the SVZ. **(B)** The cortical distribution of cIN is visualized in WT and *Kif7* -/- mouse embryos using crosses with the Nkx2.1-Cre/R26R-Tomato strain that expresses the fluorescent marker Tomato in MGE-derived cIN. Panels in B1 compare the distribution of Tomato (+) cIN in WT and *Kif7* -/- cortical sections prepared at the same rostro-caudal level and in which SVZ is immunostained with TBR2 antibodies (green). Pictures show that the deep migratory stream of

cIN terminates in *Kif7* -/- brains in the cortical region where the TBR2(+) layer reaches the cortical surface. Quantitative analysis of the mean length of the deep and superficial migratory streams measured from the entry in the pallium to the last detected cIN in the cortex is illustrated in graph B2. Statistical significance is assessed using Two way ANOVA [layers (WT, n=4; *Kif7* -/-, n=3; ***, *P*=0.001) and genotype (*, *P*=0.0157)]. **(C)** Representative pictures (C1) of the deep and superfical tangential migratory streams of cIN in the lateral cortex of WT and *Kif7* -/- embryos. Pictures illustrate the decreased thickness of the superficial stream, and the reduced distance between the deep-superficial streams in *Kif7* -/- embryos. Graph in C2 (WT, n=4; *Kif7* -/-, n=4) compares the distribution of the fluorescence intensity along a ventricle/MZ axis (see grey rectangles in C1) using the plot profile function of FIJI. Curves show no change in the distance between the ventricular wall and the deep cIN and a reduction of the distance between the two streams in the *Kif7* -/- cortical sections as quantified on the graph [WT, n=4; *Kif7* -/-, n=4; Two way ANOVA reveals a significant interaction between genotype and layer (*P*=0.0233) and multiple comparisons, a statistical difference between genotype only for the distance between de cIN streams (**, *P*=0.0051)]. Scale bars: 200 µm.

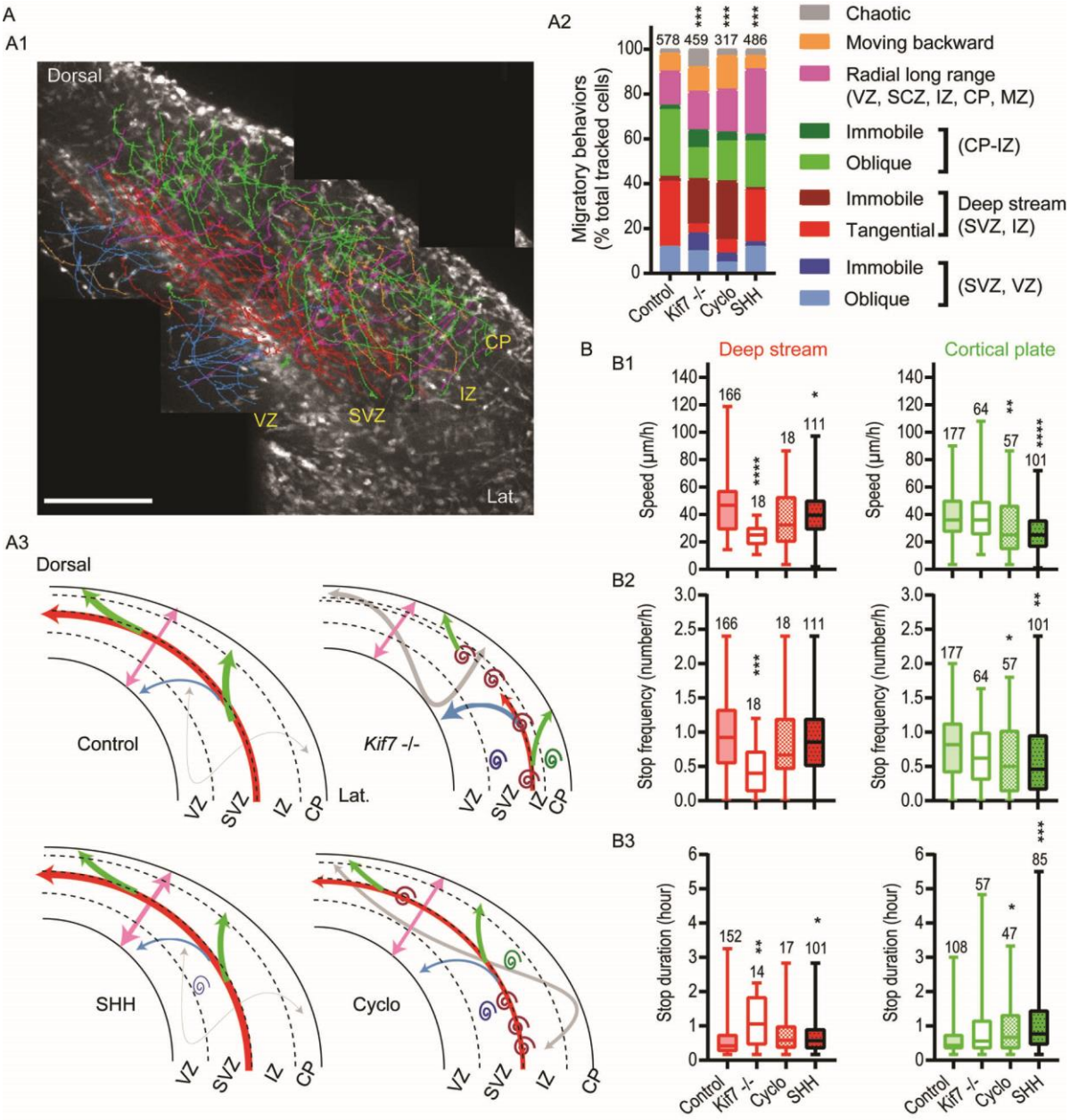

Figure 5. Dynamic behavior of migrating cIN in organotypic cortical slices: comparison between *Kif7* -/- slices and control slices with an acute treatment to either activate or block the SHH pathway. **(A)** Tomato(+) cIN migrating in living cortical slices were tracked manually using the MTrackJ plugin and their trajectories color-coded as shown in legend to characterize their preferred direction (tangential, oblique, radial, immobile) and cortical layer localization (VZ-SVZ, IZ, CP). The picture in A1 illustrates the z-projection of trajectories reconstructed in a control slice, superimposed to the last picture of the movie. Cortical interneurons migrating tangentially in the superficial migratory stream (MZ) could not be tracked because of high density. A2. Graphs compare the percentage of each kind of trajectory recorded in the lateral cortex of control slices (control, see also Suppl. Movie S3), *Kif7* -/- slices (*Kif7* -/-, see also Suppl. Movie S4), control slices treated acutely with either murine SHH

(SHH, see also Suppl. Movie S5) or cyclopamine (Cyclo, see also Suppl. Movie S6). Significance of the differences between the four distributions were assessed by a Chi-square test, X^2 (24, *n*=1224), *P*=0.0004998, ***). All experimental conditions differed from the control (Fisher test, p =0.0004998, ***). Slices from three WT animals in control condition or treated with drugs and from three *Kif7* -/- animals were analyzed; the number of analyzed cells is indicated above bars. A3. Schemes summarize the main results observed in each experimental condition. Trajectories are represented with the same color code as in A1, and line thickness is proportional to the percentage of cells exhibiting each type of trajectory. Immobile cells are figured by a coil. **(B)** Box and whisker plots indicate the mean speed (B1) and the frequency (B2) and duration (B3) of resting phases for cIN migrating tangentially in the deep stream (red box and whisker plots, left) or to the cortical plate (green box and whisker plots, right). Statistical significance assessed by Krustkal-Wallis tests in each cluster. ****, *P*<0.0001; ***, B2 left *P*=0.0005; **, B1 right *P*=0.0088, B2 right, *P*=0.0037, B3 left *P*=0.0034; *, B1 left *P*=0.0233, B2 right *P*=0.0470, B3 left *P*=0.0134, B3 right *P*=0.0394. Number of analyzed cells is indicated on plots. VZ, ventricular zone; SVZ, subventricular zone; IZ, intermediate zone; CP, cortical plate; MZ, marginal zone. Scale bar: 300 µm.

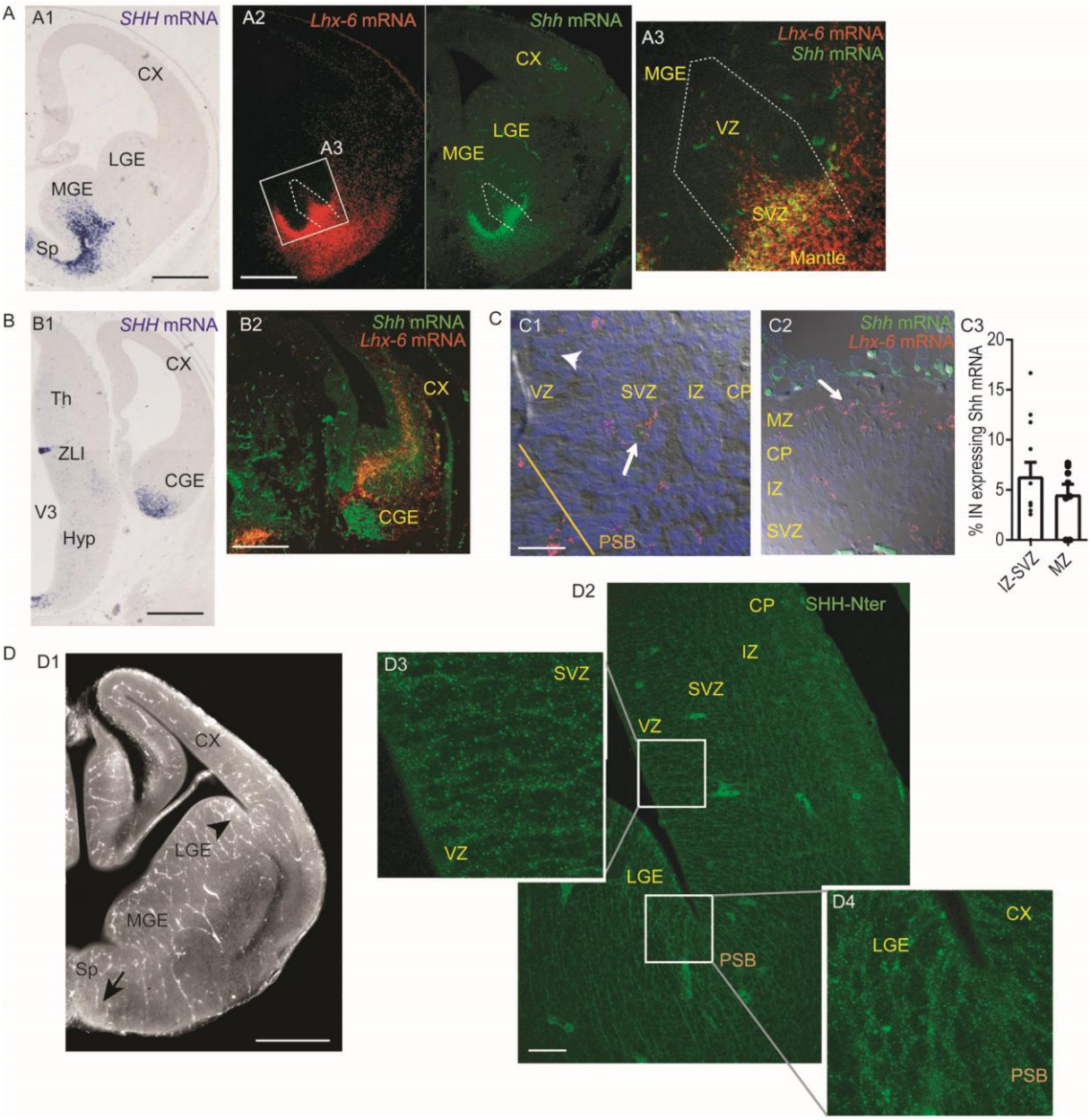

Figure 6. Expression of *Shh* transcripts (A-C) and distribution of SHH protein (D) in the developing forebrain. (A,B) Distribution in median (A) and caudal (B) coronal sections of Shh mRNA detected by *in situ* hybridization with an antisens *Shh* probe at E13.5 (A1,B1) and by RNAscope at E14.5 (A2-3,B2). *Shh* transcripts are strongly expressed in the medial ventral forebrain (SVZ and mantle zone of the MGE and septum, A1, A2), in the mantle zone of the CGE (B1,B2), in the zona limitans intrathalamica (ZLI in B1) and in the ventral midline of the 3rd ventricle (V3 in B1). RNAscope further confirmed the strong expression of *Shh* mRNA (A2, green) in MGE and septum regions that strongly express *Lhx-6* mRNA (A2, red). Confocal observations in the SVZ and mantle zone of the MGE showed that *Shh* mRNA (green) is co-expressed with the *Lhx6* mRNA (red) in a significant number of cIN (yellow cells in A3). **(C)** Confocal analyses at higher magnification of the double detection by RNAscope of *Shh* and

Lhx-6 mRNA. Cells were identified on stacked images (Δz=1 µm) using Nomarski optic. In the lateral cortex close to the PSB (C1, z projection of 10 confocal planes) and in the dorsal cortex (C2, z projection of 10 confocal planes), a very small proportion of cells expressing *Lhx-6* mRNA also express *Shh* mRNA (white arrows in C1,C2). Counting in the deep stream (SVZ-IZ) and in the MZ is shown in graph C3 (9-17 fields in three sections). A few progenitors in the cortical VZ express *Shh* mRNA at very low level (arrowhead, C1). **(D)** E14.5 forebrain coronal sections immunostained with antibodies directed against the N-ter domain of the activated SHH protein are imaged by epifluorescence (D1) and confocal (D2) microscopy. At low magnification (D1), SHH-Nter is slightly enriched in the ventral midline (black arrow) and at the ventricular angle (black arrowhead) near the PSB. Confocal analysis of SHH-Nter immunostaining (D2) shows immuno-detection in blood vessels and the presence of numerous bright dots all over the cortical neuropile. In the cortical neuropile, small bright dots align radially in the VZ (enlarged in D3), tangentially in the SVZ-IZ, and radially in the CP. On the ventricular side of the PSB and of the lateral-most part of the LGE (D3), larger SHH-Nter(+) brigth elements are aligned radially. Confocal images are a merged stacks of 10 images distant of 0.2 µm. CX, cortex; LGE, MGE and CGE, lateral, medial and caudal ganglionic eminence; V3, third ventricle; ZLI, zona intra-thalamica; Th, thalamus; Hyp, hypothalamus; PSB, pallium-subpallium boundary; VZ, ventricular zone; SVZ, subventricular zone; IZ, intermediate zone; CP, cortical plate; MZ, marginal zone. Scale bars: 500 µm (A, B, D1), 20 µm (C), 250 µm (D1), 50 µm (D2).

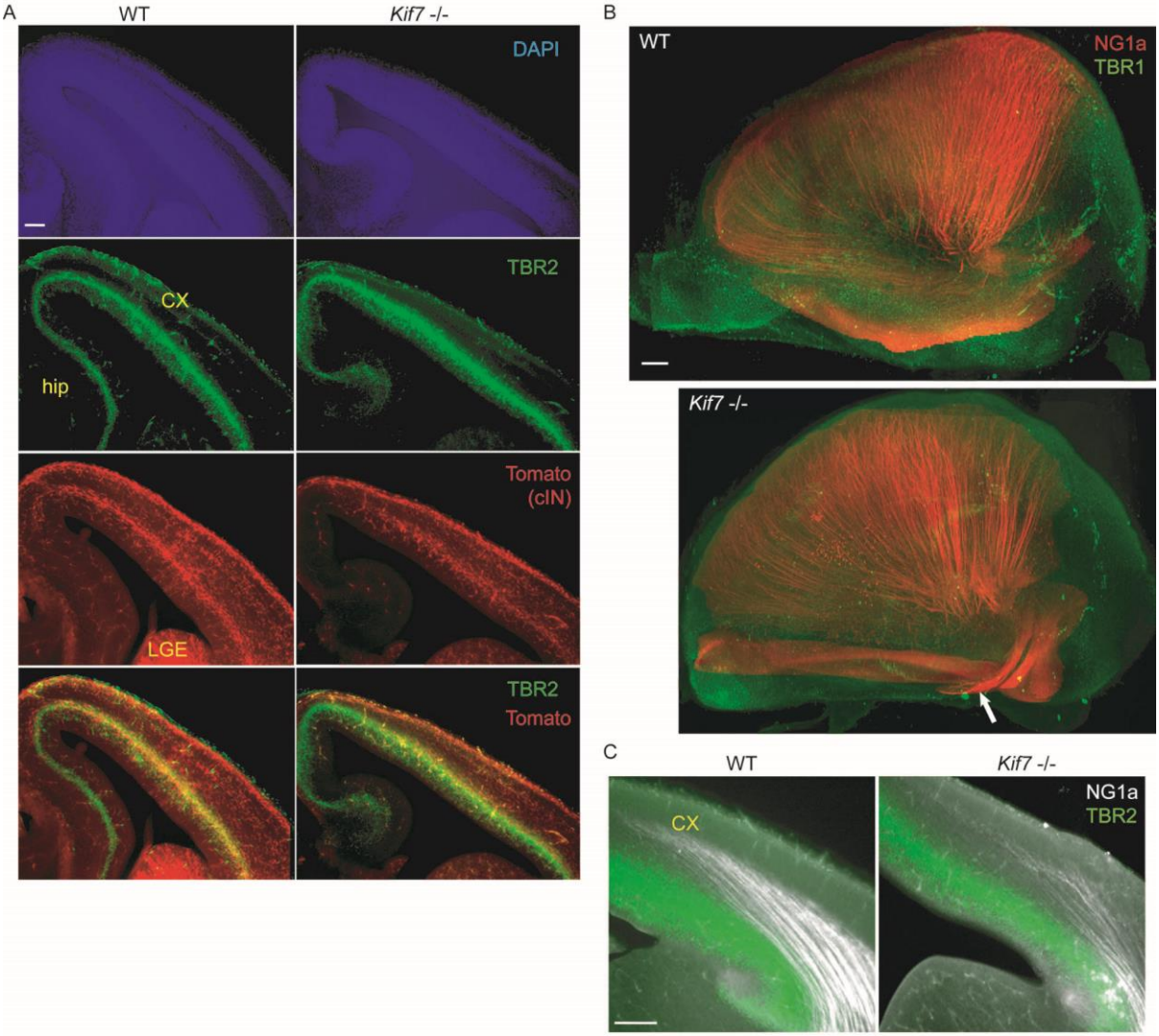

Figure 7. KIF7 deletion affects the cortex development at E16.5. (A) Coronal sections at E16.5 of transgenic Nkx2.1-Cre/R26R-Tomato control (left panels) and *Kif7* -/- (right panels) brains show that the hippocampus does not form properly in *Kif7* -/- animals and the cerebral cortex remains thinner. The migration of Tomato(+) cIN to the dorso-medial cortex had progressed between E14.5 and E16.5, but remains delayed with regard to E16.5 control brains**.** **(B)** Coronal view of whole-mount imaging of control and *Kif7* -/- brains immunostained with NG1a (red) and TBR1 (green) antibodies shows that thalamo-cortical axons extended to the cortex in both control (upper panel) and *Kif7* -/- (bottom panel) brains. An abnormal projection of thalamic axons to the ventral telencephalon is still present in *Kif7* -/- animals is (white arrow in B). **(C)** Immunostaining of thalamo-cortical axons on coronal brain sections reveals hampered colonization of the deep cortical layers above TBR2(+) layer (green) by thalamic axons (NG1a in white) in the *Kif7* -/- embryos. Scale bars: 100 µm.

SUPPLEMENTARY MATERIAL

MATERIAL AND METHODS

Brain lysate preparation and immunoblotting. Brains from WT and *Kif7* -/- were dissected at E14.5 and cortex and MGE were separately sonicated in boiling 1% SDS. Equal amounts of proteins (40 µg) were loaded on NuPAGE 4–12% Bis-Tris gels (Thermo Fisher Scientific, Waltham, MA, USA) and transferred to 0.45 µm Nitrocellulose membranes. Membranes were cut to detect signals from proteins above and below 55KDa and were blocked with 50 g/l non-fat dry milk in PBS/0.1% Tween 20 for 1h at RT, incubated with primary antibodies in the same solution O/N at 4°C, 1 h at RT with appropriate IRDye-conjugated secondary antibodies, and imaged and quantified using Odyssey Imaging System (LiCOR Biosciences, Lincolm, NE, USA). The commercial antibodies were from the following sources: anti-GLI3 (R&D Sytem-Biotechne, goat, #AF369, 1:200), anti-GAPDH (In vitrogen, mice, #AM4300, 1:2.000), Donkey-anti-goat-IR800 (Advansta, R-05781, 1:20.000), Goat-anti-mouse-IR700 (Advansta, R-05055, 1:20.000).

***In situ hybridization*.** Fixed embryos were cryoprotected overnight in PBS with 10% sucrose, embedded in OCT (Tissue-Tek, Miles, Elkhart, IN) and frozen on dry ice. 10 µm cryostat sections were thaw-mounted on Superfrost slides (Menzel-Gläser), left to dry at room temperature (RT), and stored at -80°C. Thawed sections were treated two X 10 min in RIPA buffer (150 mM NaCl, 1% NP-40, 0.5% Na deoxycholate, 0.1% SDS, 1 mM EDTA, 50 mM Tris, pH 8.0), postfixed in 4% PFA for 10 min at RT, and washed three X 5 min with PBS. The slides were then transferred in 100 mM triethanolamine, pH 8.0 for 2 min, and then acetylated for 10 min at RT by adding dropwise acetic anhydride (0.25% final concentration) while being rocked, and washed again three X 5 min in PBS. The slides were prehybridized briefly with 500 µl of hybridization solution (50% formamide, 5x SSC, 5x Denhardt's, 500 mg/ml herring sperm DNA, 250 mg/ml yeast RNA) and hybridized overnight at 70°C with the same solution in the presence of the heat-denatured DIG-labeled RNA probe. The following day, slides were washed in posthybridization solution (50% formamide, 2x SSC, 0.1% tween20) at 70°C first until coverslips slid off, then twice for 60 min at 70°C and finally at RT for 5 min. Slides were washed with buffer 1 (100 mM maleic acid, pH 7.5, 150 mM NaCl, 0.05% Tween 20), blocked for 30 min in buffer 2 (10% heat-inactivated horse serum in buffer 1), incubate overnight at 4°C with alkaline phosphatase-coupled anti-DIG antibody (Roche Diagnostics, Mannheim, Germany) diluted 1:1000 in buffer 2, rinsed twice for 5 min with buffer 1, and equilibrated for 30 min in buffer 3 (100 mM Tris, pH 9.5, 100 mM NaCl, 50 mM MgCl2). The signal was

visualized by a color reaction using 250 µl of buffer 4 per slice [6.6 µl/ml NBT (4-nitroblue tetrazolium chloride, Roche Diagnostics), 3.3 µl/ml BCIP (5-bromo-4-chloro-3-indoyl-phosphate, Roche Diagnostics) in buffer 3]. The color reaction was allowed to develop in the dark at RT during few hours and was stopped with PBS.

FIGURE AND LEGEND

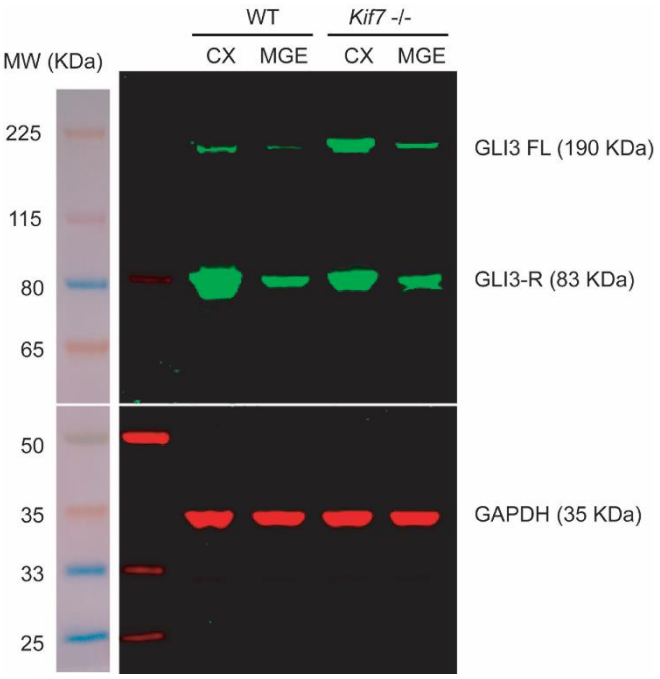

Figure S1. Western blot analysis was performed on the cortex and MGE of wild type (WT) and *Kif7* -/- embryos at E14.5. In *Kif7* -/- cortex, the clived form of GLI3 (GLI3-R at 83 KDa) was reduced as compared with control cortex whereas on the contrary, the full length GLI3 (GLI-FL at 190 KDa) was increased. The levels of GLI-FL and GLI3-R were strongly lower in the MGE compared to the cortex in WT and *Kif7* -/-. Glyceraldehyde-3-phosphate dehydrogenase (GAPDH) was used as a loading control (bottom blots).

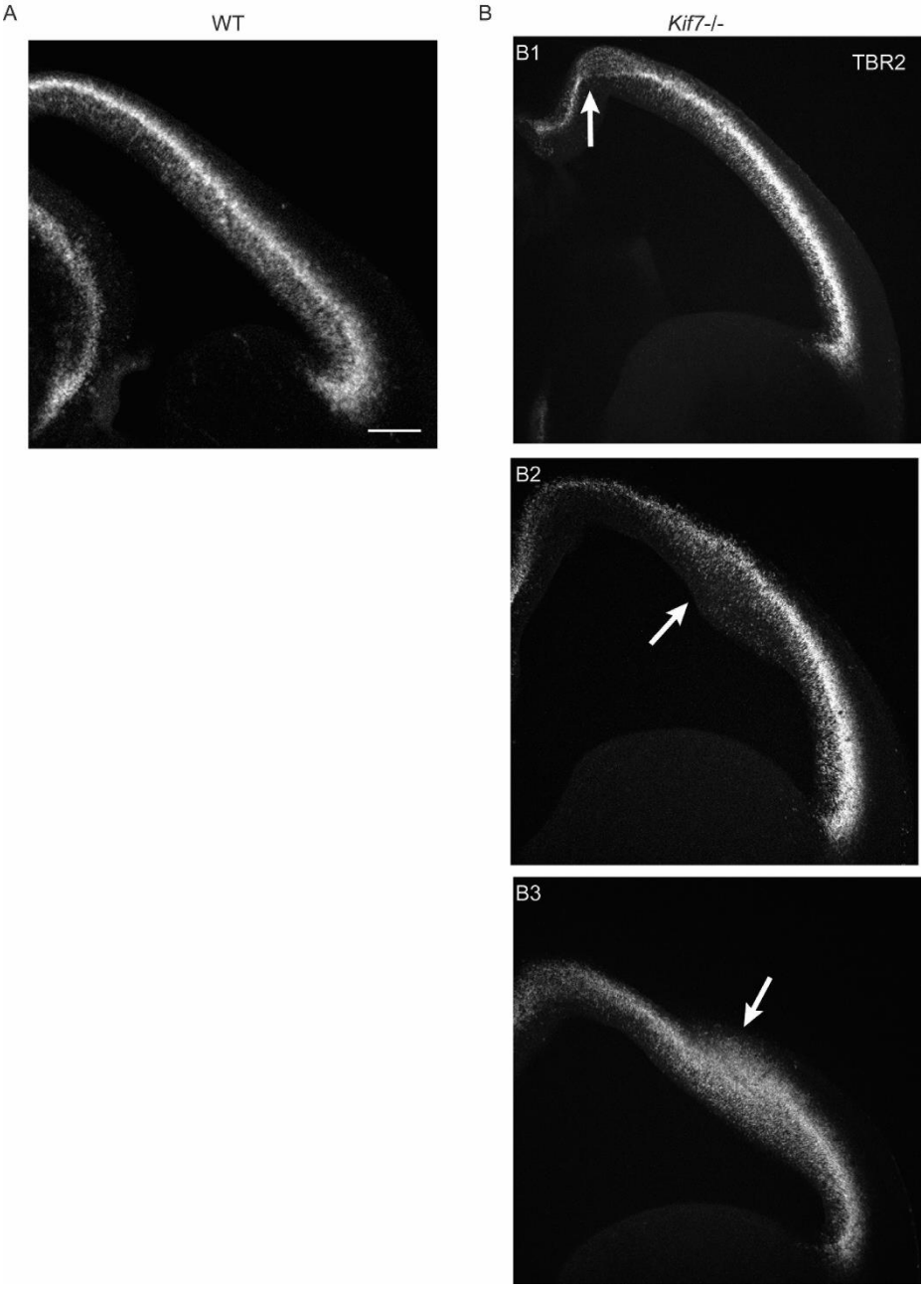

Figure S2. *Kif7* deletion is associated with cortical heterotopia at E14.5. **(A)** On coronal sections of the telencephalon of wild type (WT) animals, TBR2(+) cells form a well-defined layer restricted to the cerebral cortex. Most TBR2(+) cells are densely packed in the SVZ, whereas some TBR2(+) cells are dispersed in the ventricular zone. **(B)** In about 20% of *Kif7* -/- embryos, heterotopia identified by a disorganization of the TBR2(+) layer were observed in various regions of the cerebral cortex, either dorsal (B1) or lateral (B2,B3). Depending on heterotopia, TBR2(+) were either displaced toward the brain surface (B2) or toward the ventricle (B3). Scale bar: 200 µm.

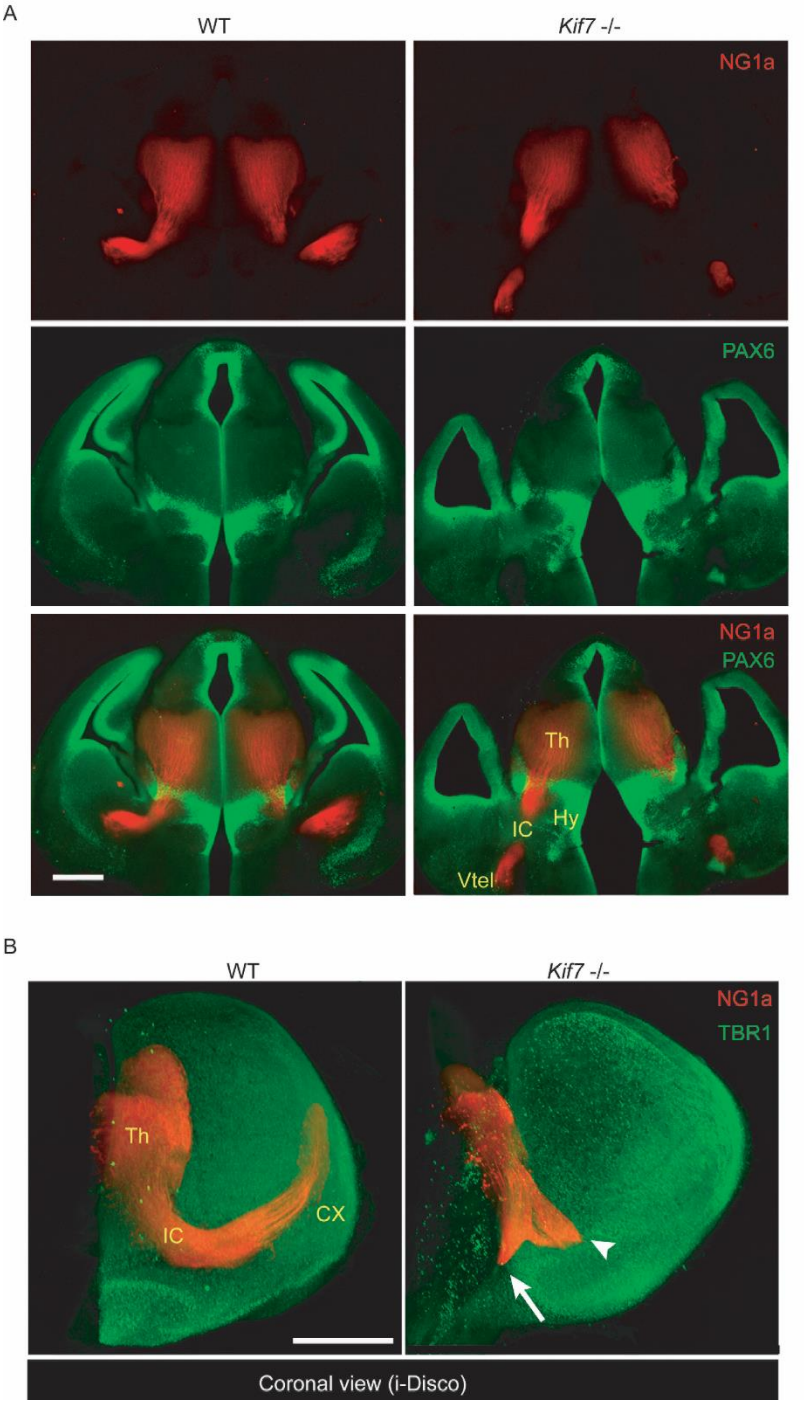

Figure S3. Alterations of the thalamo-cortical projection at E14.5 in *Kif7* -/- brains. (A) Immunostaining of coronal brain sections at a caudal level with NG1a (red) and PAX6 (green) antibodies shows that TCA mistargeting in the ventral telencephalon is not related to abnormal PAX6 expression in the zona incerta between the dorsal and ventral thalamus. **(B)** Coronal view of whole-mount imaging of transparised brains immunostained with NG1a (red) and TBR1 (green) antibodies that label respectively the thalamo-cortical projection and cortical plate cells. While all labeled thalamo-cortical axons (TCA) extend in the internal capsule (IC) and a significant proportion of them enter the cerebral cortex in the wild type brain (WT), TCA in the

Kif7 -/- brain split in two bundles in the basal telencephalon. A bundle stops shortly after entering the IC (white arrow head) whereas the second bundle extends ventrally (white arrow). Scale bar: 200 µm.

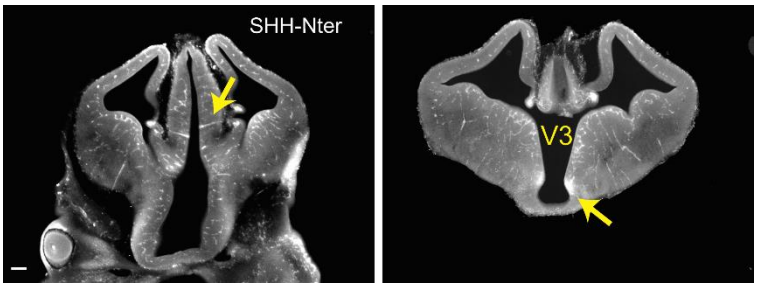

Figure S4. SHH-Nter immunostaining of brain coronal sections at E12.5. Representative pictures of SHH-Nter immunostaining imaged with a macroscope. High signal is observed in the zona limitans intrathalamica (left, arrow) and along the third ventricle (right, arrow). Scale bar: 200 µm.

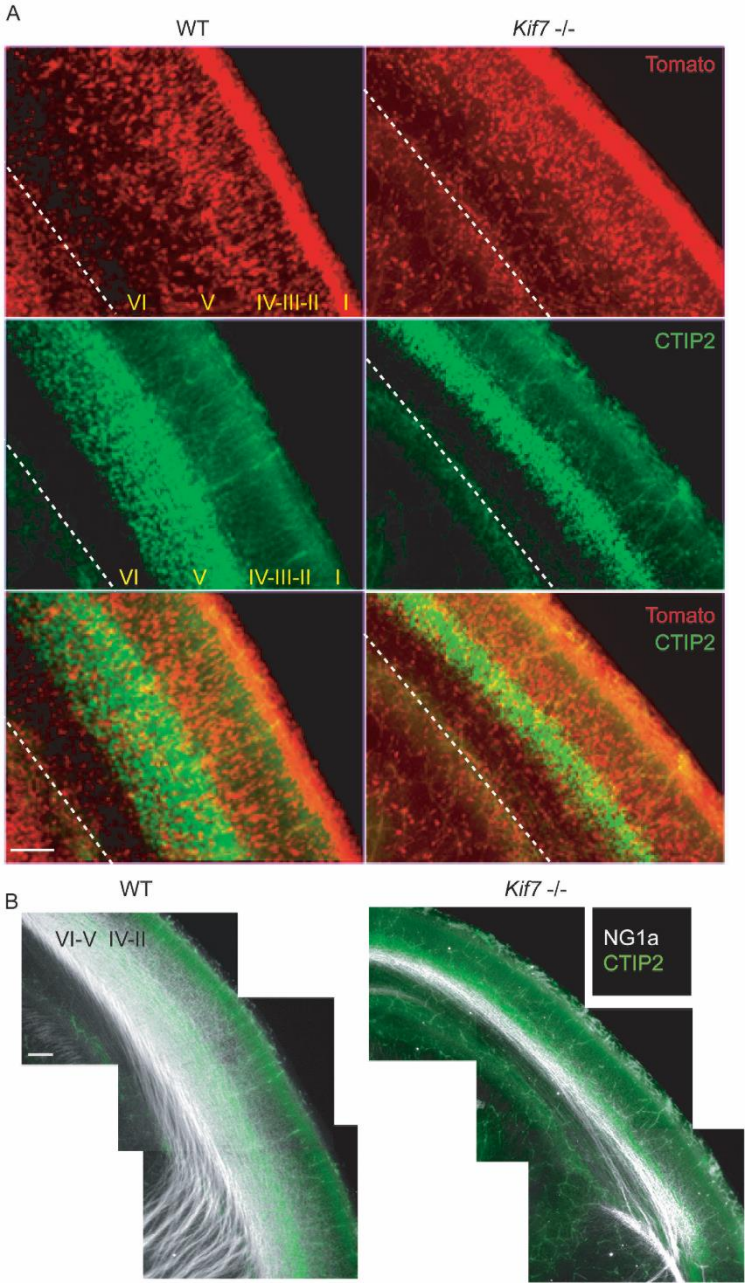

Figure S5. Kif7 deletion affects the cortex development at P0. **A.** Tomato (+) cIN are abnormally distributed in the *Kif7* -/- cortex: their density is strongly decreased in the infragranular cortical layers that express CTIP(+) principal neurons (green) and whose thickness is drastically reduced, presumably accounting for cortical thinning. **B.** Thalamo-cortical axons (TCA) labeled with NG1a antibodies (white) are able to reach the dorsal cortex in the *Kif7* -/- brain. They nevertheless appear bundled and unable to enter and colonize the cortical plate, as compared with TCA distribution in the littermate wild type brain (WT). Scale bar: 200 µm.

Movie S1 (related to Fig.3). 3D maximum intensity projection of thalamo-cortical axons in E14.5 WT brain. Whole-mount iDISCO+ immunolabeling for NG1a (in red) and TBR1(+) neurons (in green) imaged with light sheet microscopy.

Movie S2 (related to Fig.3). 3D maximum intensity projection of thalamo-cortical axons in E14.5 *Kif7* -/- brain. Whole-mount iDISCO+ immunolabeling for NG1a (in red) and TBR1(+) neurons (in green) imaged with light sheet microscopy.

Movie S3 (related to Fig.5). Migration of TdTomato expressing WT MGE cells. Forebrain slices 250 µm thick are imaged on an inverted microscope. Time-lapse between frames is 10 minutes.

Movie S4 (related to Fig.5). Migration of TdTomato expressing *Kif7* -/- MGE cells. Forebrain slices 250 µm thick are imaged on an inverted microscope. Time-lapse between frames is 10 minutes.

Movie S5 (related to Fig.5). Migration of TdTomato expressing WT MGE cells treated with mouse SHH. Forebrain slices 250 µm thick are imaged on an inverted microscope. Time-lapse between frames is 10 minutes.

Movie S6 (related to Fig.5). Migration of TdTomato expressing WT MGE cells treated with cyclopamine. Forebrain slices 250 µm thick are imaged on an inverted microscope. Time-lapse between frames is 10 minutes.